JOURNAL OF PETROLOGY | VOLUME 47 | NUMBER 6 | PAGES 1119–1146 | 2006 | doi:10.1093/petrology/egl005

Trace Element and Sr–Pb–Nd–Hf Isotope Evidence for Ancient, Fluid-Dominated Enrichment of the Source of Aldan Shield Lamproites

G. R. DAVIES[1]*, A. J. STOLZ[2], I. L. MAHOTKIN[3], G. M. NOWELL[4] AND D. G. PEARSON[4]

[1]FACULTY OF EARTH AND LIFE SCIENCES, VRIJE UNIVERSITEIT, DE BOELELAAN 1085, 1081 HV AMSTERDAM, THE NETHERLANDS

[2]MAX-PLANCK-INSTITUT FÜR CHEMIE, ABT. GEOCHEMIE, POSTFACH 3060, 55020 MAINZ, GERMANY

[3]INSTITUTE OF ORE DEPOSITS (IGEM), RUSSIAN ACADEMY OF SCIENCE, STAROMONETNY 35, MOSCOW 109017, RUSSIA

[4]DEPARTMENT OF GEOLOGICAL SCIENCES, DURHAM UNIVERSITY, SOUTH ROAD, DURHAM DH1 3LE, UK

RECEIVED JUNE 23, 2003; ACCEPTED JANUARY 26, 2006
ADVANCE ACCESS PUBLICATION MARCH 7, 2006

A phase of Mesozoic extension associated with the termination of continental collision at the southern margin of the Aldan Shield produced ultrabasic lamproites in a discontinuous belt 500 km long and ~150 km wide. The lamproites, locally poorly diamondiferous, were emplaced as dykes, sills and pipes. All Aldan lamproites have primitive chemical characteristics (e.g. MgO up to 22·7 wt %) and are ultrapotassic (K_2O up to 8·3 wt %) and peralkaline with $K_2O + Na_2O/Al_2O_3$ in the range 0·6–1·16. A distinctive feature of these rocks is their low TiO_2 content (0·5–1·4 wt %). Aldan lamproites are moderately light rare earth element (LREE) enriched with $(La/Yb)_N$ ranging from 10 to 47. Heavy rare earth element (HREE) abundances are lower than for all other lamproites by up to a factor of five. Therefore, the combined major and trace element characteristics of the Aldan samples are not typical of other lamproite occurrences. Large ion lithophile element concentrations are high (100–800 × Primitive Mantle) but the high field strength elements (HFSE; Nb, Ta, Ti) plus Th and U display unusually low concentrations for rocks of this type. The style of trace element enrichment recorded by the Aldan Shield lamproites is comparable with that of subduction-related magmatism. The Aldan lamproites have among the most extreme initial isotopic ratios yet recorded from mantle-derived magmas; $\varepsilon_{Ndi} = -10·3$ to $-22·3$, $^{87}Sr/^{86}Sr_i = 0·7055–0·7079$, $\varepsilon_{Hfi} = -7·6$ to $-29·4$ and $^{206}Pb/^{204}Pb_i = 16·6–17·4$. When interpreted in terms of multi-stage Pb isotope evolution, the Pb isotope data require fractionation from a Bulk Earth reservoir at 3·0 Ga and subsequent evolution with second-stage μ values between 6·4 and 8·0. The inferred Archaean age of the lamproite source is consistent with Nd and Hf model ages, which range from 1·5 to 3·0 Ga. Aldan lamproites have $\Delta\varepsilon_{Hf}$ values that range from +3 to −7. Trace element and Sr–Nd–Pb–Hf isotopic ratios show coherent variations that suggest that Archaean source enrichment produced the negative $\Delta\varepsilon_{Hf}$ as a result of metasomatism by slab-derived hydrous melts that left rutile–garnet-bearing residua. We conclude that relatively large degrees of partial melting produced the lamproites (>5%), which explains the preservation of the isotope–trace element correlations and the low REE contents. Although high-quality trace element data (e.g. HFSE) are not available for most lamproites, it appears that many of their source regions contain a component of recycled oceanic crust, possibly including subducted sediment. The sources of the Aldan and many other lamproites are distinct from ocean island basalt mantle sources. This suggests that the long-term storage of trace element enriched lamproite sources occurred in the sub-continental lithospheric mantle and not at depth within the convecting asthenosphere.

KEY WORDS: *potassic volcanism; isotope geochemistry; fluid enrichment*

*Corresponding author. Fax: 31-205989942. E-mail: gareth.davies@falw.vu.nl

INTRODUCTION

Continued improvement in our understanding of melt extraction processes has produced a general consensus that porous flow, melt–residue interaction and melt channelling all play important roles in magma genesis. Despite this consensus, the major processes that control the generation of potassic volcanic rocks remain strongly debated (Edgar & Mitchell, 1997; Turner *et al.*, 1999; Janney *et al.*, 2002; Nowell *et al.*, 2004). Deeply derived ultramafic rocks such as kimberlites and ultrapotassic rocks such as lamproites represent the most extreme incompatible element-enriched products of mantle melting. These rocks can have K_2O contents of up to 12 wt % (Foley *et al.*, 1987). All workers agree that the parental magmas of such rocks cannot be derived from the asthenospheric upper mantle in a single-stage process and that highly incompatible element enriched sources are required (e.g. see reviews by Bergman, 1987; Foley *et al.*, 1987). Many variants of multi-stage models have been proposed (e.g. Smith, 1983; Fraser *et al.*, 1985; Nelson *et al.*, 1986; Turner *et al.*, 1999; Nowell *et al.*, 2004). One model argues that the sources of the most extreme trace element enriched magmas, such as lamproites and Group II kimberlites, reside in the parts of the sub-cratonic lithospheric mantle (SCLM) that have been heavily modified by metasomatic processes (e.g. Smith, 1983; Fraser *et al.*, 1985; Nelson *et al.*, 1986; Murphy *et al.*, 2002). The origin of the metasomatic melts is ascribed to small degrees of partial melting within the asthenosphere (Fraser *et al.*, 1985) or subduction-related processes that include a significant sedimentary component (Nelson *et al.*, 1986). An alternative model proposes that lamproites and kimberlites are derived from sub-lithospheric mantle depths and represent the surface manifestation of the passage of a mantle plume beneath the area. The plume source is argued to contain a component of recycled lithospheric material (e.g. Le Roex, 1986; Janney *et al.*, 2002; Murphy *et al.*, 2002). In an attempt to resolve this long-running debate a detailed geochemical and isotopic study has been conducted of Mesozoic lamproitic magmatism in eastern Siberia.

REGIONAL GEOLOGY

The Siberian Craton (Fig. 1) occupies an area of about 4×10^9 km^2. Most of the craton is buried beneath 1–8 km of Riphean–Phanerozoic sedimentary cover. To the north and east, the craton is in contact with the predominantly sedimentary basins of the Phanerozoic foreland (Taimyr and Verkhoyansk Belts). Orogenic belts (Palaeozoic Central Asian and Mesozoic Mongolo-Okhotsk) occur in the north and in the west. Exposures of crystalline basement are restricted to regions of tectonic uplift and make up <30% of the surface exposure. Based on surface geology and the interpretation of geophysical data, the Siberian Craton appears to be formed from a series of accreted microcontinents bounded by major shear zones (e.g. see Rosen *et al.*, 2002, for review). Five such provinces are recognized: Tungus, Anabar, Olenek, Aldan and Stanovoi. They are composed of diverse tectonic blocks (terranes) and include Early Proterozoic orogenic fold belts. Geochronological evidence suggests that there were major crust-forming events within the Siberian Craton at 3·5, 3·3, 3·0 and 2·5 Ga (Rosen *et al.*, 2002). Indirect evidence in support of an Archaean age for the Siberian Craton comes from dating of samples derived from the lithospheric mantle. Siberian eclogite and diamondiferous peridotite xenoliths and syngenetic peridotite inclusions in diamonds have yielded Re–Os ages of 3·5 to 3·1 Ga (Pearson *et al.*, 1995, 1999). The major amalgamation of the Siberian Craton occurred in two Palaeoproterozoic collision events that are approximately dated at 1·9 and 1·8 Ga (Rosen *et al.*, 2002). The sedimentary cover demonstrates that the Siberian Platform was a peneplain by the beginning of the Riphean (1·65 Ga), i.e. within 150 Myr of the previous major tectono-magmatic activity.

The Aldan Shield forms the southern part of the Siberian Platform (Fig. 1; Bilanenko *et al.*, 1984; Perchuk *et al.*, 1985; Jahn *et al.*, 1998). The Aldan–Stanovoi terranes are characterized by complex structures caused by several tectono-magmatic events resulting from successive accretion of different orogenic belts and cratons to the Aldan and Tynda terranes. The accretion events occurred during the period from 2·1 to 1·7 Ga (Popov & Smelov, 1996; Rosen *et al.*, 2002). The Precambrian Aldan Shield now comprises three distinct blocks: (1) Archaean granite–greenstone terranes in the west (Olekma Block); (2) Early Archaean (3·3 Ga) gneissic granulites and granites of the Central Block; (3) amphibolites intercalated with granulites of the Timpton Block in the east (Popov & Smelov, 1996). The last major accretion event in the region occurred in the Mesozoic when the Burein Block, which experienced extensive reworking in the Proterozoic, was added from the south.

NOMENCLATURE OF ULTRAPOTASSIC ROCKS

The extreme petrographic diversity of ultrapotassic rocks has led to confusing definitions, classification and nomenclature. Consequently, petrographically and compositionally similar rocks sometimes have been given different names, e.g. the madupites of the Leucite Hills are similar to the jumillites of SE Spain. The discovery of diamondiferous ultrapotassic rocks in the Kimberley

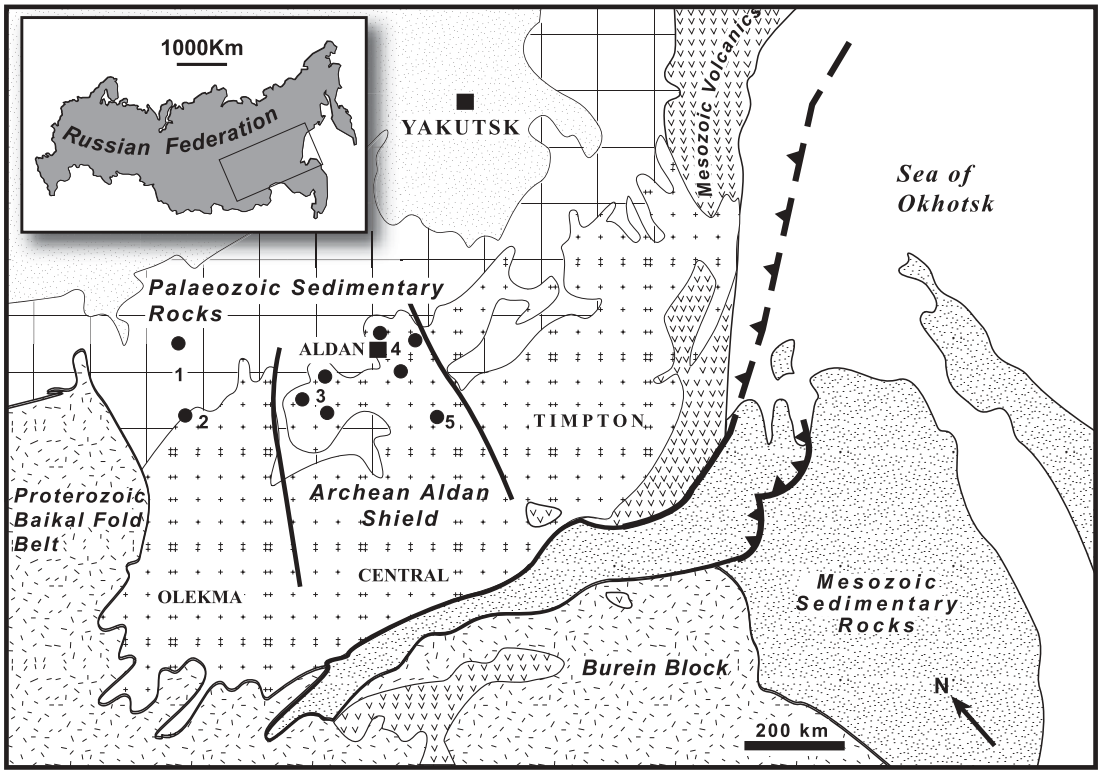

Fig. 1. Generalized geological sketch map of Eastern Siberia, after Rosen *et al.* (2002), showing the major tectonic units and sampling locations. Inset map shows the position of Eastern Siberia in relation to the territory of the Russian Federation. Major tectonic sutures are marked by bold black lines. The Aldan Shield is subdivided into three terranes: Olekma, Central and Timpton. Scattered Mesozoic volcanic rocks crop out across all of Eastern Siberia and only the major occurrences are shown. Major lamproite occurrences are indicated by filled circles: 1, Molbo; 2, Murun; 3, Chompolo; 4, Central Aldan area (Nizhni-Yokokut, Verhni-Yokokut); 5, Loman.

region of Western Australia in the 1970 s led to renewed interest in these rock types and ultimately to a better consensus over nomenclature (Scott Smith & Skinner, 1984; Bergman, 1987; Foley *et al.*, 1987; Mitchell & Bergman, 1991). Rocks are defined as ultrapotassic if they have K_2O/Na_2O weight ratios >2 and K_2O >3 wt %. In addition, the term is usually restricted to mafic rocks, i.e. those with MgO >3 wt %. Typical compositional criteria are molar K_2O/Al_2O_3 ratios >0·8 and $(K_2O + Na_2O)/Al_2O_3$ >0·7. Typically, CaO and FeO_T are <10 wt % and incompatible trace element contents are high; Ba >2000 ppm, Sr >1000 ppm and La >100 ppm. Mitchell & Bergman (1991), however, argued that the term lamproite should not be defined solely on the basis of geochemistry and that a combination of mineralogical and geochemical criteria is needed. The chemical compositions of ultrapotassic rocks fall into three end-member groups: lamproites, kamafugites (group II) and plagioleucites of the Roman Province (group III) (Fig. 2; Foley *et al.*, 1987).

Lamproites occur in continental settings, often marginal to cratonic areas, but are rare, known from ~20 major suites worldwide (Bergman, 1987). Lamproites have highly variable occurrences ranging from dykes and sills to flows, cinder cones, diatremes and pyroclastic deposits. The misidentification of olivine lamproites from the USA and Western Australia as kimberlites is evidence that there are similarities between the two rock groups. There are, however, numerous petrological and compositional differences. The main petrological characteristics of lamproites are:

(1) modal proportions of phlogopite and richterite, fosteritic olivine, diopside and sanidine are high;
(2) olivine phenocrysts in lamproites often form complex crystal aggregates of euhedral grains compared with the isolated anhedral macrocrysts found in kimberlites;
(3) minor phases include leucite, enstatite, priderite, wadeite, apatite, kerroite and armalcolite; carbonate, ilmenite and rutile are rare.

These mineralogical characteristics are a consequence of lamproites having higher SiO_2, TiO_2, P_2O_5, BaO and particularly K_2O than kimberlites. Lamproites are also characterized by lower Al_2O_3, CaO, MgO, FeO_T and volatiles (H_2O, CO_2).

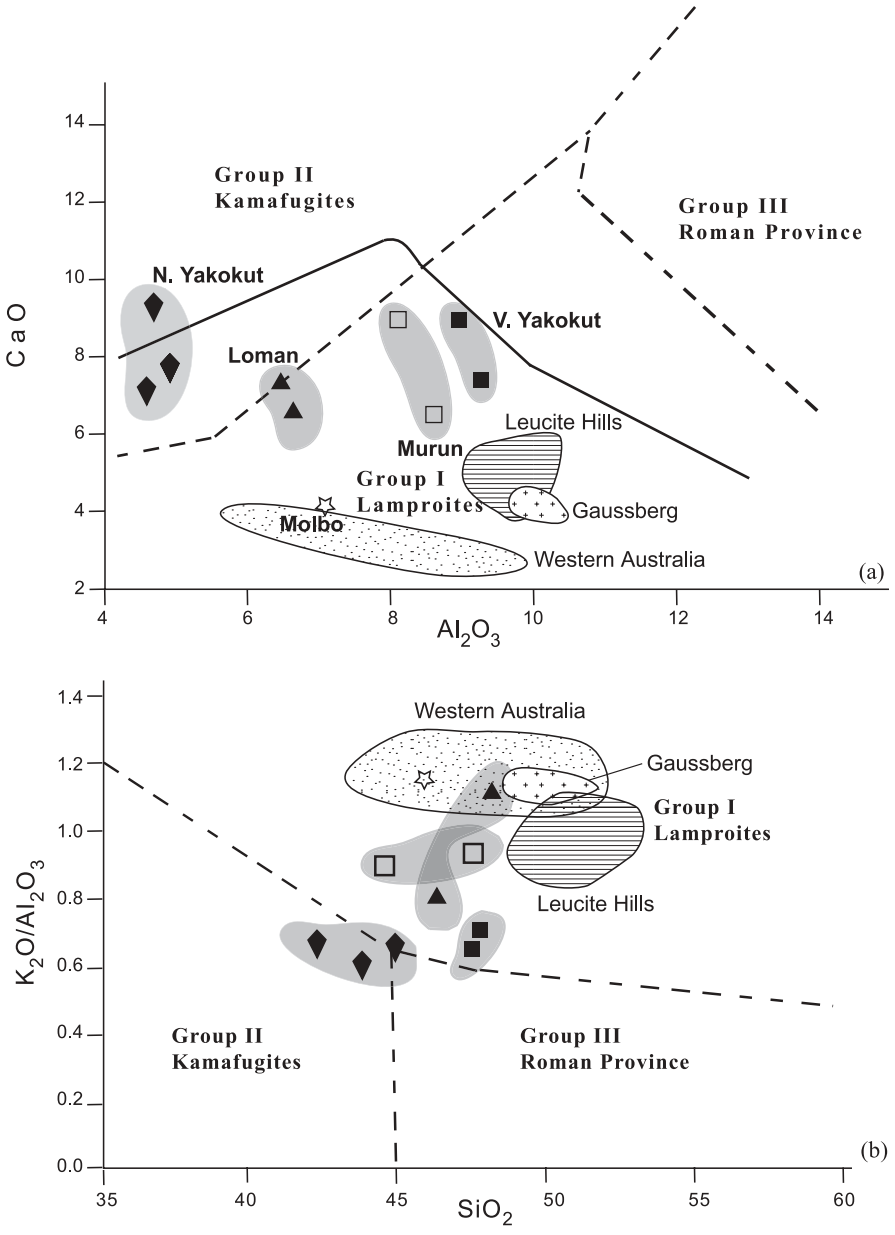

Fig. 2. Major element variation diagrams of (a) CaO vs Al_2O_3 and (b) K_2O/Al_2O_3 vs SiO_2. Ultrapotassic rocks can be subdivided into three main groups based on their major element compositions: continuous line indicates Group I, lamproites; dashed lines indicate Group II, kamafugites, and Group III, Roman Province (Foley *et al.*, 1987). Fields for Western Australian, Gaussberg and Leucite Hills lamproites are plotted for comparison (Fraser *et al.*, 1985; Mitchell & Bergman, 1991; Murphy *et al.*, 2002).

ALDAN LAMPROITES

Regional occurrence and terminology

Mafic and ultramafic lamproites of Mesozoic age are widespread, but volumetrically small, in the northern part of the Aldan Shield (Fig. 1; Bogatikov *et al.*, 1985; Mahotkin *et al.*, 1989; Meus-Schumacher *et al.*, 1995; Vladykin, 1997). In total, alkaline igneous rocks cover an area of ~150 km^2 (Vladykin, 1996). Evidence of the Mesozoic magmatism is preserved in a discontinuous belt 500 km long and ~150 km wide, located 500 km north of the Mesozoic collision zone. Details of the regional geological setting and mineralogy of the Aldan lamproites have been reported previously by various workers (e.g. Mues-Schumacher *et al.*, 1995; Panina, 1997; Vladykin, 1997). Only the most pertinent features are, therefore, summarized here. The ultrapotassic magmatism is closely associated with other mafic and ultramafic volcanic rocks. There appears to be a temporal progression from subalkaline (~180 Ma, minettes, syenites, trachytes and

monzonites) to potassic (~ 150 Ma, leucitites, phonolites and alkaline syenites and granites) and ultimately to ultrapotassic lamproite magmatism (143–122 Ma).

The basic–ultrabasic ultrapotassic rocks of the Aldan Shield have been defined as lamproites on the basis of their bulk-rock major element composition (e.g. Bogatikov *et al.*, 1985) and that most of their constituent minerals have compositions comparable with those of lamproites elsewhere in the world (Panina, 1997). Mitchell *et al.* (1994), however, have argued that some rock types are orthoclase–kalsilite pyroxenites and shonkinites, and that these ultrapotassic rocks are members of the biotite pyroxenite–shonkinite suite. In addition, the low TiO_2 contents of the Aldan lamproites and the absence of Ba–Ti–Zr-bearing minerals (e.g. priderite, wadeite, lindsleyite, etc.) are not typical of lamproites. The term lamproite, however, has been used extensively in both the Russian and western literature to describe the ultrapotassic rocks from the Aldan Shield (e.g. Bogatikov *et al.*, 1985; Mahotkin *et al.*, 1989; Mues-Schumacher *et al.*, 1995; Panina, 1997; Vladykin, 1997). Therefore, despite the fact that the rocks are not lamproites *sensu stricto*, the term lamproite is used throughout this paper to avoid confusion.

Relatively low-temperature processes have extensively altered the vast majority of Aldan lamproites. Locally, however the, glassy groundmass and olivine phenocrysts are preserved. Sampling was confined to these unaltered lamproite occurrences, which unfortunately means that sample availability for this study was limited.

Central Block occurrences

The lamproites occur in two broad areas. In the Central Aldan Block lamproites of 143–136 Ma occur in clusters near Chompolo, Loman and three regionally associated occurrences termed Nizhni-Yakokut, Yakokut Alkaline Massif and Verhni-Yakokut. These lamproites were emplaced in the form of sills (1–3 m thick), dykes (1–20 m thick) and pipes. One pipe from the Nizhni-Yakokut volcanic field is poorly diamondiferous and contains mantle-derived peridotite xenoliths. An alkaline complex, locally called the Yakokut Alkaline Massif, is located ~25 km SE of the town of Aldan in the Central Aldan Block. The massif covers an area of ~20 km^2 and contains numerous olivine–clinopyroxene lamproite dykes 1–3 m thick. The massif itself mainly comprises alkaline and quartz syenites but is surrounded by shonkinites, leucitites, pseudoleucitites and phonolites (Mahotkin *et al.*, 1989; Mues-Schumacher *et al.*, 1995). The lamproite dykes intrude both intrusive and extrusive rock types but are more concentrated in the south of the complex where extrusive rocks are more common. The dykes contain xenoliths of dunite, shonkinite and wehrlite. The Loman Massif is located ~150 km SE of Aldan. The massif comprises a variety of lamproites, shonkinites and alkaline syenites (Vavilov *et al.*, 1986). To the west of the Loman Massif there is a major occurrence of alkaline granites and syenites. Olivine–clinopyroxene lamproites from the Verhni-Yakokut region form layered sills, 1–60 m thick. Locally the bases of the sills are olivine enriched so that bulk-rock compositions are not always representative of magmatic compositions. Dykes occur over an area of ~25 km and intrude Archaean basement gneisses. Dyke orientations generally follow lineations in the basement.

The least altered dykes from the Central Block were sampled from the Nizhni-Yakokut, Verhni-Yakokut and Loman occurrences. The lamproites are olivine, diopside, phlogopite and Cr-spinel phyric with a cryptocrystalline matrix. The rocks are highly porphyritic with rounded or euhedral phenocrysts of both olivine and diopside, which form between 15 and 40% of the rock. The abundance of phlogopite phenocrysts is more variable (3–25%). Olivine and diopside phenocrysts are highly magnesian (Mg-number 88–95). Coupled with the high Cr-number of the spinels (85–96), these mineral compositions suggest derivation of the magmas from a depleted mantle source. The groundmass assemblages consist of diopside + phlogopite ± pseudoleucite ± sanidine + oxides and altered glass. The phenocryst abundances and the major groundmass minerals are reported in Table 1.

Olekma Block occurrences

Lamproites in the Olekma Block (133–122 Ma, Murun and Molbo) occur principally as dykes. There are two major mineralogical differences from the lamproites of the Central Block. First, richteritic amphibole is a common phenocryst phase. Second, generally the rocks have lower abundances of olivine and diopside and lower Mg-number (88–90). More extensive petrographic descriptions have been given by Mahotkin *et al.* (1989), Mues-Schumacher *et al.* (1995), Panina (1997) and Vladykin (1997).

The Little Murun Complex crops out in the Olekma Block ~350 km WNW of Aldan. The Complex is ~15 km^2 in extent and includes four distinct suites of alkaline rocks (Vladykin, 1997; Mitchell *et al.*, 1994). The south of the complex comprises the Charoite carbonatite. The core of the Little Murun Complex comprises potassic syenites. Alkaline trachytes and leucite phonolite lavas and tuffs make up the NW part of the complex. The NE part of the complex is formed of clinopyroxenites, kalsilite pyroxenites (yakutites) and shonkinites. Lamproites form dykes and sills, up to 20 m thick, and flows throughout most of the complex. The lamproites include olivine–clinopyroxene ± leucite, leucite–clinopyroxene–richterite, richterite–sanidine and

Table 1: Mineralogy and abundance of phenocrysts in the Aldan Lamproites

Sample	Rock type	Phenocryst phases					
		Olivine	Diopside	Phlogopite	K-richterite	Pseudoleucite	Sanidine (after leucite)
Nizhni–Yakokut							
424/85	olivine–phlogopite–pyroxene lamproite	35 + m	5 + m	m		m	m
495/85	olivine–phlogopite–pyroxene lamproite	30 + m	5 + m	m		m	m
116/84	olivine–phlogopite–pyroxene lamproite	30 + m	5 + m	m		m	m
Verhni–Yakokut							
19/86	olivine–pyroxene–phlogopite lamproite	15	10 + m	m		m	m
101/86	olivine–pyroxene–phlogopite lamproite	15	10 + m	m		m	m
Loman							
126/86	olivine–phlogopite–pyroxene lamproite	30	30	5 + m		m	m
127/86	olivine–phlogopite–pyroxene lamproite	25	30	5 + m		m	m
Murun							
132/86	olivine–phlogopite–pyroxene lamproite	20	20 + m	10 + m		m	m
136/86	K-richterite–phlogopite–sanidine lamproite	2	7 + m	20 + m	15	m	m
Molbo							
68/88	olivine–clinopyroxene–leucite mafic lamproite	5	2	m		10	m

Phenocryst abundances are given as percentages and the presence of a phase in the groundmass is indicated by m.

clinopyroxene–leucite varieties. The Molbo River lamproite crops out ~150 km north of the Little Murun Complex. The studied olivine–clinopyroxene–leucite lamproite forms a 1·5 m thick dyke with chilled margins that intrudes late Cambrian sediments (Panina, 1997). The phenocryst abundances and the major groundmass minerals of the Olekma Block samples are reported in Table 1.

ANALYTICAL TECHNIQUES

Major elements and several trace elements (Cr, Ni, Sc, V) were analysed with a Philips PW1400 X-ray fluorescence spectrometer at Institute of Ore Deposits (IGEM) in Moscow. The majority of trace element data were determined by spark source mass spectrometry (SSMS) at the Max-Planck-Institut für Chemie (MPI) in Mainz. Details of the analytical methods, precision and accuracy of the SSMS technique have been given by Jochum *et al.* (1990). Individual elements are better than ±7% and element ratios are better than ±5%. Lu and Hf were determined by inductively coupled plasma mass spectrometry (ICP-MS) at the Vrije Universiteit, Amsterdam on an HP 4500plus system following standard procedures (Eggins *et al.*, 1997).

Throughout the text, errors in isotopic ratios are given as 2 standard deviations of the mean for standard analyses and 2 standard errors of the mean for individual analyses. Sr–Nd isotope ratios were determined at the Vrije Universiteit, Amsterdam following standard ion exchange separation techniques (Heumann & Davies, 2002). Sr samples were loaded onto single annealed Re filaments with $TaCl_5$. Sr isotope ratios were measured dynamically using a Finnigan MAT 261 system and corrected for mass fractionation following an exponential law based on $^{86}Sr/^{88}Sr = 0{\cdot}1194$. During the course of analyses, the mean value for NBS 987 was $0{\cdot}710245 \pm 10$ ($n = 12$). Nd isotope ratios, determined as a metal species, were measured dynamically using a Finnigan MAT 262 system and corrected for mass fractionation following an exponential law based on $^{146}Nd/^{144}Nd = 0{\cdot}7219$. During the course of analyses, the mean value for our CIGO internal standard was $0{\cdot}511342 \pm 7$ ($n = 18$). On the basis of >200 analyses of both the CIGO standard and the La Jolla international standard, the CIGO value equates to 0·511844 for La Jolla.

Pb isotope analyses were undertaken at the MPI. Sample powders (~100 mg) were dissolved in Savilex beakers using a mixture of concentrated HNO_3 and HF. The Pb chemistry followed a similar procedure to that of White & Dupre (1986) and involved separation of the Pb in 100 µl anionic resin exchange columns using a combination of HBr and HCl elutions. The total procedural Pb blank was ~80 pg. At MPI all isotopic analyses were determined on a Finnigan MAT261 multi-collector mass spectrometer in static mode. Lead isotope ratios were corrected for mass fractionation by ~0·07% per a.m.u., based on repeated analyses of

NBS981 run at the same temperature as unknowns. All samples were measured twice and the analyses represent averages with the reproducibility of the measurements generally being better than 0·03% per a.m.u.

Hf isotopes were determined at Durham University using a ThermoFinnigan Neptune plasma ionization multi-collector mass spectrometer (PIMMS). Details of PIMMS analytical techniques and chemical separation of Hf have been given by Nowell *et al.* (2003). $^{176}Hf/^{177}Hf$ ratios were corrected for mass fractionation following an exponential law based on $^{179}Hf/^{177}Hf = 0{\cdot}7325$. During the course of analyses (2 days) multiple measurements of the international Hf standard JMC475 gave $0{\cdot}282146 \pm 8$ ($n = 27$). All Hf data are normalized to the accepted value of JMC475 of 0·282160 (Nowell *et al.*, 1998*b*).

ε_{Hf} values were calculated using $^{176}Hf/^{177}Hf$ and Lu/Hf ratios for a chondritic uniform reservoir (CHUR) from Blichert-Toft & Albarède (1997). Delta ε_{Hf} ($\Delta\varepsilon_{Hf}$) is defined as the difference between the measured (or initial) Hf isotope ratio and that predicted from the oceanic basalt Nd–Hf isotope correlation line of Vervoort *et al.* (1999). The correlation line is defined as $\varepsilon_{Hf\,(OIB)} = 1{\cdot}33\varepsilon_{Nd} + 3{\cdot}19$ (where OIB is ocean island basalt).

RESULTS

Major and trace element data

The lamproites all display primitive chemical characteristics with high MgO (up to 22·7 wt %), Cr and Ni contents and Mg numbers. Although some of the olivine phenocrysts in the most Mg-rich samples are likely to be of cumulate origin, their high Mg-numbers (88–94·6) indicate that they crystallized from Mg-rich primitive magmas. The ultrapotassic character of these Mg-rich rocks is reflected by the high K_2O (up to 8·3 wt %), low Na_2O (mostly $\leq$1·5 wt %) and high K_2O/Na_2O weight ratios (3–9). The rocks are peralkaline with $(K_2O + Na_2O)/Al_2O_3 = 0{\cdot}6$–$1{\cdot}16$. SiO_2 contents are in the range 42·4–48·1 wt % and Al_2O_3 4·9–9·2 wt %. The Aldan lamproites have somewhat higher CaO and relatively low Al_2O_3 contents (Fig. 2) compared with many other lamproites, particularly those from Spain (Venturelli *et al.*, 1984) and the Kimberley region of Western Australia (Jaques *et al.*, 1986). Consequently, although most of the Aldan samples fall in the field for lamproites, there is some overlap with kamafugites in diagrams of Al_2O_3 vs CaO and K_2O/Al_2O_3 vs SiO_2 (Fig. 2; Foley *et al.*, 1987). Perhaps the most distinctive feature of the major and minor element chemistry of these rocks is their low TiO_2 contents (0·5–1·4 wt %), which are lower than those of almost all other lamproitic rocks including the Spanish (Venturelli *et al.*, 1984). In a number of samples the low TiO_2 concentrations are coupled with low P_2O_5 (0·25–0·7 wt %).

When major element compositions are plotted on Harker variation diagrams (not shown) there is no evidence of a major influence by fractional crystallization or crustal contamination (e.g. trends to higher SiO_2). The possible exception are the samples from Murun and Molbo with the lowest MgO contents (7·3 and 8·5 wt %; Mg-number 57 and 66, respectively) that have lower SiO_2 and Al_2O_3 and higher TiO_2 contents (Table 2). Accumulation or fractional crystallization of the major phenocryst phases could potentially cause marked fractionation in major element ratios. For example, richterite and clinopyroxene addition could lower K_2O/CaO, whereas phlogopite addition would increase this ratio. In contrast, olivine addition will only dilute K_2O contents and not change K_2O/CaO significantly. The major element data do not suggest that olivine fractionation or accumulation is the dominant contributor to the major element variations of the Aldan lamproites. Some of the major element variation (Table 2) could be ascribed to fractionation or accumulation of richterite and clinopyroxene. Lamproites worldwide, however, record a large range in ratios such as K_2O/Al_2O_3 and K_2O/CaO, which suggests that these ratios are, at least partly, source controlled. We conclude that, because of the extreme compositions of lamproites and the limited number of unaltered samples available for study, it is difficult to determine unambiguously the role of fractional crystallization and phenocryst accumulation. With the exception of the two most evolved lamproite samples, there appears no compelling evidence of major accumulation or loss of the observed phenocryst phases. Generally high Ni and Cr contents and poor correlations with MgO support this conclusion (Table 2). This uncertainty, however, does not significantly affect the conclusions reached later in the paper, as detailed petrogenetic arguments will be predominantly based on isotopic and incompatible trace element data.

The lamproites are generally characterized by high concentrations of the compatible trace elements Cr and Ni, but only moderate Sc and V concentrations compared with typical alkaline basaltic rocks. Some of the incompatible K-group elements (e.g. Rb, Ba and Pb) also occur in high concentrations, but the high field strength elements (HFSE; Ti, Zr, Nb and Hf), plus Th, U and the light rare earth elements (LREE; La, Ce) display unusually low concentrations for lamproites. These differences are illustrated in Fig. 3, where primitive mantle normalized trace element diagrams clearly demonstrate the overall lower trace element contents of the Aldan samples compared with typical lamproites worldwide. The Aldan samples exhibit several significant differences from other lamproites. Chondrite-normalized REE patterns for the Aldan lamproites (Fig. 4) contrast markedly

Table 2. Major and trace element compositions of the Aldan Shield lamproites

	Central Block							Olekma Block		
Sample:	424/85	495/85	116/84	19/86	101/86	126/86	127/86	132/86	136/86	68/88
Age (Ma):	143	143	143	136	136	122	122	133	133	120
Location:	Nizhni-Yakokut	Nizhni-Yakokut	Nizhni-Yakokut	Verhni-Yakokut	Verhni-Yakokut	Loman	Loman	Murun	Murun	Molbo
SiO_2	43·84	44·97	42·38	47·59	47·76	45·97	48·12	44·77	47·10	46·40
TiO_2	0·54	0·48	0·58	0·62	0·71	0·91	1·39	1·01	1·02	1·25
Al_2O_3	4·91	4·63	4·60	8·79	9·18	6·47	6·94	8·66	8·16	7·15
Fe_2O_3	6·82	6·18	8·67	4·81	4·70	3·60	3·01	5·15	4·39	11·34
FeO	5·93	4·88	3·66	4·05	5·26	5·37	3·33	5·19	4·84	1·22
MnO	0·18	0·16	0·17	0·17	0·14	0·14	0·05	0·13	0·20	0·11
MgO	22·70	21·43	21·96	14·00	13·86	21·25	18·70	14·25	8·52	7·29
CaO	7·61	9·16	6·87	9·06	7·61	7·33	7·02	6·55	8·98	4·22
Na_2O	0·74	0·92	0·72	1·52	1·48	0·77	0·91	1·50	2·57	1·19
K_2O	2·90	3·10	3·09	5·94	5·72	5·20	8·04	7·58	7·55	8·26
P_2O_5	0·50	0·33	0·54	0·57	0·73	1·11	0·25	1·91	0·32	2·22
H_2O	1·34	1·36	2·29	0·50	1·23	0·23	0·97	0·40	1·07	5·16
CO_2	0·53	1·19	2·90	0·79	0·22	0·20		0·92	3·22	1·00
F	0·13	0·17	0·08	0·15	0·20	0·35	0·86	0·91	0·51	0·25
Sum	98·89	98·96	98·51	98·56	98·80	98·90	99·59	98·93	98·60	97·15
Mg-no.	79	81	79	77	75	83	86·2	75	66·2	57·3
Sc			21·5	22·2	25·5	20·8	25·2	21·8		17
V	185	157		150	196	185	157	213	340	840
Cr	590	670	1515	1100	630	1160	1180	1030	270	110
Co	99	86	91	56	52	62	42	50	39	34
Ni	700	630		470	360	900	73	190	120	92
Rb	87	151	104	288	129	177	235	314	268	164
Sr	912	681	998	561	1893	1123	727	3145	3844	4139
Y	11·1	8·9	13·9	13·1	16·5	12	5·21	20	36	30·5
Zr	50·0	41·4	58·3	107·5	253	32·3	43·6	113·9	261	403
Nb*	2·30	1·43	2·22	3·53	4·98	1·87	2·48	7·61	15·39	25·11
Sn†	0·475	0·543	1·71	0·798	3·35	0·37	1·472	3·17	3·25	5·59
Sb†	0·475	0·21	0·277	0·095	2·136	0·044	0·068	0·373	0·317	1·41
Cs†	3·25	5·11	2·52	4·66	3·14	3·8	4·08	5·15	3·08	0·505
Ba	2441	1234	2903	2745	2548	2071	1269	2250	7991	12773
La	13·88	9·18	15·40	28·82	21·1	34·81	9·04	53·2	66	68·1
Ce	38·38	24·43	37·1	63·27	51·71	98·11	28·92	100·6	137·58	190·83
Pr	4·47	2·57	3·97	6·57	6·45	12·17	3·54	11·45	13·23	20·84
Nd	17·07	9·85	13·38	27·48	24·91	40·39	15·69	42·12	52·79	75·31
Sm	3·68	2·54	3·51	5·81	5·67	6·42	4·1	9·68	10·18	12·89
Eu	1·082	0·823	1·00	1·946	1·529	2·45	0·818	2·355	2·67	2·89
Gd	3·08	2·70		5·61	4·73	4·97	2·87	6·82	6·99	7·43
Tb	0·489	0·469		0·92	0·7	0·752			1·05	0·787
Dy	2·33	1·78	1·95	4·68	3·14	3·9	1·395	3·85	4·46	3·62
Ho	0·382	0·313	0·387	0·731	0·486	0·64	0·202	0·569	0·693	0·523
Er	1·011	0·782	0·992	1·813	1·155	1·414	0·482	1·367	1·305	1·358
Tm	0·145	0·116	0·116	0·181	0·195	0·125	0·065	0·173		0·14
Yb	0·853	0·624	0·760	1·01	0·771	0·758	0·413	1·126	0·85	0·90
Hf†	1·63	1·25	1·63	3·03	5·34	1·03	1·16	3·05	6·09	9·58

	Central Block							Olekma Block		
Sample:	424/85	495/85	116/84	19/86	101/86	126/86	127/86	132/86	136/86	68/88
Age (Ma):	143	143	143	136	136	122	122	133	133	120
Location:	Nizhni-Yakokut	Nizhni-Yakokut	Nizhni-Yakokut	Verhni-Yakokut	Verhni-Yakokut	Loman	Loman	Murun	Murun	Molbo
Lu†	0·120	0·108	0·119	0·163	0·237	0·142	0·061	0·178	0·346	0·251
Ta*	0·157	0·088	0·143	0·236	0·277	0·125	0·163	0·491	0·910	1·403
Tl†	0·923	1·159	0·724	0·68	0·831	0·522	0·271	2·76	2·24	0·164
Pb‡	55·8	14·2	24·9	7·33	26·4	5·41	5·31	3·53	62·4	84
Bi†	0·098	0·02	0·041	0·011	0·087	0·035	0·01	0·022	0·285	0·185
Th‡	2·086	2·092	2·924	2·573	3·891	0·875	0·789	6·48	6·2	12·51
U‡	1·116	0·786	1·333	1·123	1·422	0·325	0·208	3·3	1·6	5·65

Major elements were determined by XRF except for F, and CO_2 and H_2O, which were determined by wet chemistry techniques. Trace elements were determined by XRF unless otherwise stated. All REE were determined by ICP-MS at Amsterdam.
*Determined by SSMS.
†Determined by ICP-MS at Amsterdam.
‡Determined by isotope dilution.

with those of all other lamproites, including the relatively Ti-poor Spanish lamproites. The La/Yb_N ratios of Aldan samples are low (9·8–47) compared with values for other lamproites, which are typically >100. Heavy REE (HREE) abundances (e.g. Yb = 0·4–1·1 ppm) are also lower than those of other lamproites by between factors of two and five (Fig. 4). Moreover, the Aldan samples have no Eu anomaly that is a characteristic of, for example, the Ti-poor Spanish lamproites.

In addition to lower trace element contents, the style of trace element enrichment of the Aldan lamproites is distinct from that of other lamproite occurrences. The large ion lithophile element (LILE) enrichment approaches that of other lamproites, with Pb, K, Sr and Cs contents being comparable with those of the Western Australian lamproites. In marked contrast, the Aldan samples exhibit strong relative depletion (or lack of enrichment) of the HFSE and LREE. The most notable features are the pronounced relative depletion of Nb and Ta. Other HFSE elements (Zr, Hf and Ti) are only moderately enriched compared with primitive mantle and markedly less so than other lamproites. For example, Hf concentrations in most lamproites are in the range 25–50 ppm (e.g. Fraser *et al.*, 1985) compared with 1–10 ppm for the Aldan samples. Many lamproites are characterized by minor HFSE depletion compared with elements of a similar degree of incompatibility and this is reflected in high La/Nb and K/Nb ratios (e.g. Western Australia 0·6–2·3 and 200–700, respectively). In contrast, the Aldan samples record extreme fractionation, with La/Nb and K/Nb ratios of 4·2–18·6 and 2700–27 000, respectively. The Aldan Shield lamproites, therefore, have trace element characteristics that are widely regarded as diagnostic of subduction-related magmatism and have a trace element signature similar to that of highly potassic rocks from subduction-related tectonic settings (e.g. olivine leucitite from Indonesia; Stolz *et al.*, 1990; van Bergen *et al.*, 1992; Gertisser & Keller, 2003).

Hf, Nd, Sr and Pb isotopes

In a $^{87}Sr/^{86}Sr$ vs $^{143}Nd/^{144}Nd$ diagram (Fig. 5), the Aldan lamproites plot outside the range of present-day OIB and are characterized by very unradiogenic Nd ($\varepsilon_{Ndi} = -10{\cdot}3$ to $-22{\cdot}3$) and, when compared with Bulk Earth, moderately radiogenic Sr ($^{87}Sr/^{86}Sr_i$ = 0·7055–0·7079). Several samples from the Central Aldan Block fall within the field for lamproites from the Leucite Hills at low $^{143}Nd/^{144}Nd$ ratios and the remainder plot within, or close to, the field for Smoky Butte lamproites (Fraser *et al.*, 1985). These suites contrast with the Spanish, Gaussberg and Western Australian lamproites, which have much more radiogenic Sr and slightly more radiogenic Nd isotope compositions (Fig. 5). The Nd–Sr isotopic relationships indicate that the lamproite sources have variable Rb/Sr, with the source of the Aldan and North American (Leucite Hills, Smoky Butte) lamproites recording moderate time-integrated Rb/Sr enrichment.

Despite the well-preserved nature of the Aldan samples studied here, there is always the possibility that low-temperature alteration processes have played a role in producing the observed Sr isotope compositions. In addition, despite the high trace element contents of these

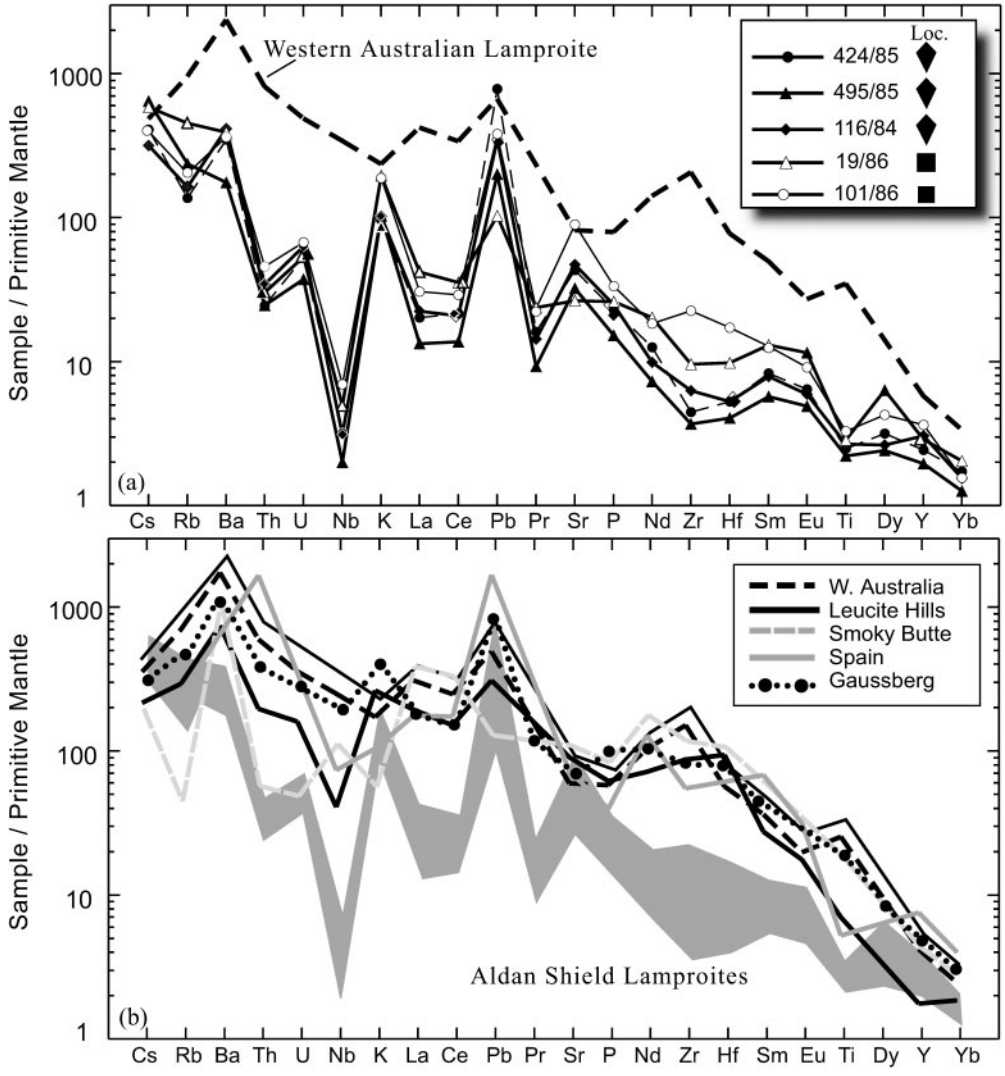

Fig. 3. Trace element abundances in lamproites normalized to primitive mantle values (Sun & McDonough, 1989). (a) Representative lamproite samples from the Aldan Shield (Nizhni-Yokokut, Verhni-Yokokut and Loman occurrences compared with a typical lamproite from Western Australia. (b) Representative lamproites from Western Australia, Leucite Hills, Smoky Butte, Spain and Gaussberg compared with the range of Aldan Shield lamproites (data sources: Nixon *et al.*, 1984; Fraser *et al.*, 1985; Nelson *et al.*, 1986; Mitchell & Bergman, 1991; Turner *et al.*, 1999; Murphy *et al.*, 2002). Symbols for individual normalized trace element patterns have no significance; location symbols are as for Fig. 2.

samples, there is always a possibility that large amounts of contamination by isotopically extreme Archaean crust could have influenced the isotopic compositions of the rocks. Clinopyroxene separates were, therefore, analysed from six samples to assess the importance of any late-stage magmatic or low-temperature processes. The Sr isotope data are reported in Table 3. The close similarity in initial Sr isotope ratios clearly demonstrates that the whole-rock data have not been significantly modified since clinopyroxene crystallization. We therefore conclude that low-temperature alteration and extensive crustal interaction have not affected the Aldan lamproites.

Hf isotope compositions are also very variable ($\varepsilon_{Hfi} = -7{\cdot}6$ to $-29{\cdot}4$, Table 2) and record a larger range than OIB (Fig. 6). The lowest initial ratios are among the most unradiogenic values measured for mantle-derived magmatic rocks to date. Partial melting in the mantle is thought to lead to a coupled fractionation in Sm/Nd and Lu/Hf ratios such that present-day oceanic and subduction-related volcanism and average continental crust form a well-defined linear relationship between Nd and Hf isotopes. The majority of the Aldan lamproites lie on, or close to, an extension of the oceanic array at less radiogenic values than Group II kimberlites (Fig. 6; Nowell *et al.*, 1999). Departure from the oceanic array can be expressed in terms of the parameter $\Delta\varepsilon_{Hf}$ (Beard & Johnson, 1993; Fig. 7). The lamproites from the Aldan Shield plot just above, to well below, the oceanic

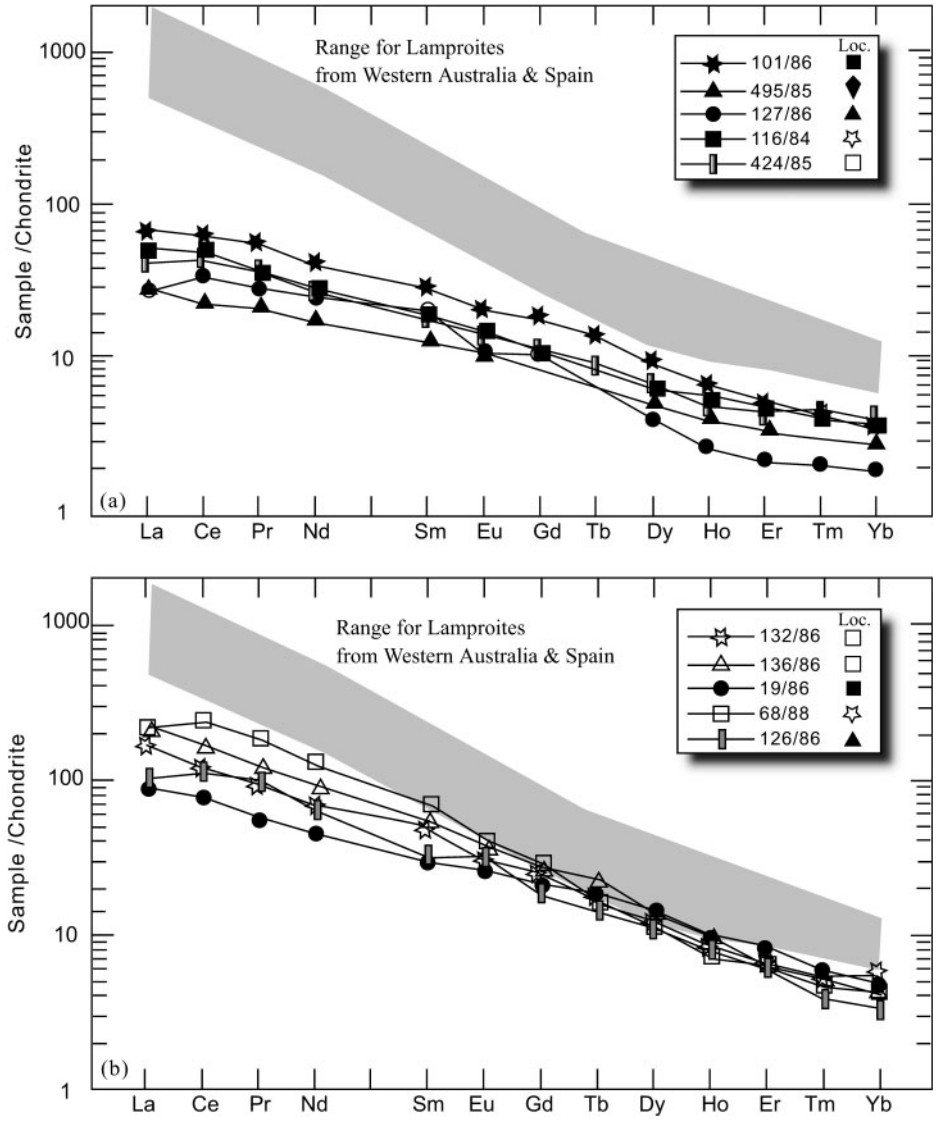

Fig. 4. Chondrite-normalized REE patterns for lamproite normalization values from Sun & McDonough (1989). (a) Lamproites from Nizhni-Yokokut, Verhni-Yokokut and Loman; data are from Table 2. Symbols for individual normalized trace element patterns have no significance; location symbols are as for Fig. 2. (b) Samples from Verhni-Yokokut and Loman, Molbo and Murun. Shaded fields encompass the range of lamproites from Western Australia and Spain (data sources: Nixon *et al.*, 1984; Fraser *et al.*, 1985; Nelson *et al.*, 1986).

array (MORB–OIB, where MORB is mid-ocean ridge basalt), with $\Delta\varepsilon_{Hf}$ +3·4 to −7·3 (Fig. 7). Lamproites from other localities worldwide have more negative $\Delta\varepsilon_{Hf}$ values but similar ε_{Ndi} (Nowell *et al.*, 1998*a*), demonstrating that all lamproites are derived from mantle sources characterized by very long-term LREE enrichment and low Lu/Hf. The predicted temporal evolution of 1% non-modal batch partial melts from both spinel and garnet lherzolites is plotted in Fig. 7, along with the predicted evolution of recycled enriched (E)- and normal (N)-MORB, for comparison with the lamproite data.

The Aldan lamproites all have unradiogenic $^{206}Pb/^{204}Pb_i$ and plot close to, or to the left of, the geochron on a $^{206}Pb/^{204}Pb$ vs $^{207}Pb/^{204}Pb$ isotope diagram (Fig. 8a). This is in contrast to the majority of MORB, OIB and other K-rich rocks from New South Wales, Africa and Spain. The Pb isotope ratios of the Aldan rocks fall in two discrete fields that overlap with the Leucite Hills–NW Colorado and Smoky Butte lamproites (Fraser *et al.*, 1985). The two distinct populations plot above and below the Northern Hemisphere Reference Line (NHRL) defined by the majority of Atlantic oceanic (MORB and OIB) magmatism (Hart, 1984). The more radiogenic group has Pb isotope compositions that overlap the Indian MORB field whereas the second group has significantly less radiogenic $^{206}Pb/^{204}Pb$ and

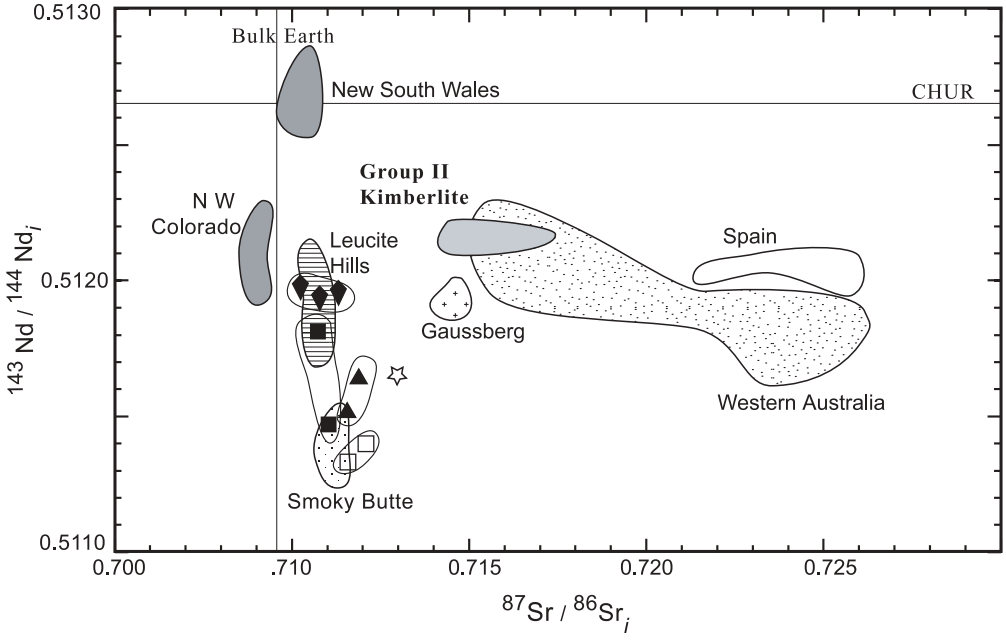

Fig. 5. Initial Sr–Nd isotope ratios of Aldan Shield lamproites, southern African Group II kimberlites and examples of worldwide lamproites. Data sources: McCulloch *et al.* (1983); Smith (1983); Nixon *et al.* (1984); Fraser *et al.* (1985); Smith *et al.* (1985); Nelson *et al.* (1986); Mitchell & Bergman (1991); Nelson (1992); Rogers (1992); Wannamaker *et al.* (2000); Davies *et al.* (2001); Murphy *et al.* (2002).

$^{207}Pb/^{204}Pb$. The relationships between the two groups are similar in the $^{206}Pb/^{204}Pb$ vs $^{208}Pb/^{204}Pb$ diagram (Fig. 8b), with the Aldan rocks overlapping, in part, the field for Leucite Hills lamproites. The group with the more radiogenic $^{206}Pb/^{204}Pb$ ratios has $^{208}Pb/^{204}Pb$ ratios comparable with Indian MORB. However, the group of Aldan lamproites with the lowest $^{206}Pb/^{204}Pb$ values has higher $^{208}Pb/^{204}Pb$ values than the Smoky Butte lamproites and is significantly more radiogenic than the NHRL. This suggests that the mantle source had higher time-integrated Th/Pb and Th/U values than the source of the Smoky Butte lamproites.

DISCUSSION

The aim of this paper is to constrain the processes responsible for the distinctive trace element and isotopic signature of the Aldan lamproites. This requires that the effect of any source trace element enrichment (metasomatism) can be distinguished from any trace element fractionation associated with melt extraction and any subsequent magmatic or low-temperature alteration processes. In addition, we aim to assess if lamproite mantle sources are located entirely within the SCLM, or are sub-lithospheric, possibly related to the activity of mantle plumes (i.e. similar sources to that of OIB).

Age of source enrichment

The Aldan Shield lamproites appear to be highly primitive magmas with high Sr and Pb concentrations. Consequently, we have followed the reasoning of previous workers (e.g. Fraser *et al.*, 1985; Nelson, 1992) who have argued that the trace element and isotopic signature of the lamproites has been little affected by crustal contamination and that their isotopic compositions are a good proxy of the mantle source region. Although this conclusion has been questioned in some cases (e.g. Nowell *et al.*, 2004) we rule out a significant role for crustal contamination and low-temperature alteration in producing the observed incompatible trace element and isotopic compositions of the Aldan lamproites because of:

(1) their primitive major and trace element characteristics;
(2) the moderately high incompatible trace element contents of the rocks, which makes them insensitive to these processes;
(3) the occurrence of diamonds and peridotitic mantle xenoliths, which demonstrates that the lamproites were emplaced rapidly from mantle depths;
(4) Sr isotope equilibrium between clinopyroxene separates and host whole-rocks (Table 3).

The isotopic and geochemical characteristics of the Aldan lamproites are, therefore, ascribed to mantle processes.

Despite the effects of parent/daughter ratio fractionation during the partial melting event that produced the Aldan lamproites, calculated depleted mantle model ages for Nd and Hf are consistently ancient in the range 1·5–3·0 Ga. The coupled Sr–Nd–Hf isotope

Table 3: Sr–Nd–Hf isotope compositions of whole-rock and clinopyroxene separates of the Aldan Shield lamproites

Sample	Location	Age (Ma)	Sm	Nd	$^{143}Nd/^{144}Nd_m$	$^{143}Nd/^{144}Nd_i$	$\varepsilon_{Nd\ i}$	Rb	Sr	$^{87}Sr/^{86}Sr_m$	$^{87}Sr/^{86}Sr_i$	Lu	Hf	$^{176}Hf/^{177}Hf_m$	$^{176}Hf/^{177}Hf_i$	$\varepsilon_{Hf\ i}$	$\Delta\varepsilon_{Hf}$
424/85	1	143	3·68	17·07	0·512011 ± 9	0·51189	−11·0	87	912	0·706276 ± 9	0·70572	0·142	1·030	0·282496 ± 9	0·282465	−7·6	3·36
424/85 cpx								11·5	748	0·705752 ± 9	0·70566						
495/85	1	143	1·196	3·984	0·512071 ± 8	0·51193	−10·28	151	681	0·706800 ± 6	0·70550	0·061	1·371	0·282448 ± 5	0·282415	−9·4	0·67
495/85 cpx								18·7	554	0·705726 ± 8	0·70553						
116/84	1	143	3·51	16·12	0·512057 ± 7	0·51193	−10·6	104	998	0·706448 ± 6	0·70584	0·163	2·739	0·282496 ± 8	0·282466	−7·6	2·89
116/84 cpx								11·3	798	0·705903 ± 7	0·70582						
19/86	2	136	5·81	27·48	0·511546 ± 8	0·51143	−20·1	288	561	0·708887 ± 6	0·70602	0·120	1·509	0·282115 ± 8	0·282093	−20·9	1·86
19/86 cpx								34·2	421	0·706485 ± 8	0·70601						
101/86	2	136	5·67	24·91	0·511938 ± 8	0·51182	−12·6	129	1893	0·706154 ± 8	0·70577	0·119	1·532	0·282140 ± 9	0·282121	−19·9	6·87
126/86	3	122	6·195	24·32	0·511647 ± 9	0·51157	−17·73	177	1123	0·707742 ± 6	0·70695	0·237	4·654	0·282240 ± 12	0·282012	−17·7	2·07
126/86 cpx								12·5	1035	0·707002 ± 8	0·70694						
127/86	3	122	7·119	27·29	0·511777 ± 8	0·51166	−15·91	235	727	0·708298 ± 7	0·70668	0·178	3·147	0·282189 ± 5	0·282194	−18·4	1·00
127/86 cpx								21·7	587	0·706841 ± 8	0·70666						
132/86	4	133	9·68	42·12	0·511447 ± 9	0·51135	−21·77	314	3145	0·707681 ± 8	0·70713	0·346	6·088	0·281993 ± 9	0·282174	−25·3	0·26
136/86	4	133	10·18	52·79	0·511507 ± 8	0·51141	−20·67	268	3844	0·707545 ± 7	0·70716	0·251	9·389	0·281876 ± 8	0·281972	−29·4	5·84
68/88	5	120	12·88	75·31	0·511768 ± 8	0·51169	−15·5	164	4139	0·708131 ± 8	0·70794	0·108	1·270	0·282021 ± 7	0·281855	−24·2	7·29

m, measured ratios; i, initial ratios. Sample locations as in Fig. 1: 1, Nizhni-Yakokut; 2, Verhni-Yakokut; 3, Loman; 4, Murun; 5, Molbo.

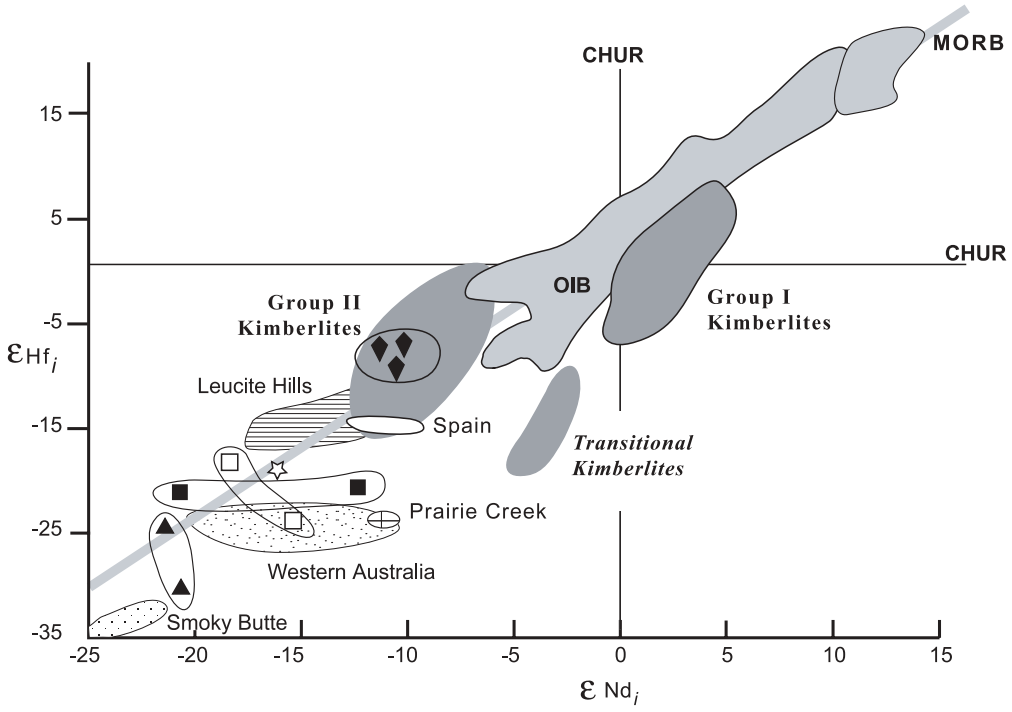

Fig. 6. Initial Nd–Hf isotope ratios (expressed in ε notation) of Aldan Shield lamproites compared with MORB and OIB worldwide. Also shown for reference are fields for southern African Group I and II and Transitional kimberlites and examples of lamproites worldwide from Nowell *et al.* (1998*a*, 2004). Comprehensive references to representative MORB and OIB data sources have been given by Nowell *et al.* (1998*b*) and Vervoort *et al.* (1999). The 'mantle array' (grey line) is a linear regression ($\varepsilon_{Hf} = 1{\cdot}33\varepsilon_{Nd} + 3{\cdot}19$) through MORB and OIB; data are from Vervoort *et al.* (1999).

characteristics, therefore, suggest that the Aldan lamproites were derived from a mantle source characterized by very long-term relative LREE enrichment and moderate Rb/Sr enrichment.

The Aldan Shield lamproites were sampled from localities over 500 km apart and record marked source isotopic heterogeneity. The Pb isotope data, for example, define two distinct clusters ($^{206}Pb/^{204}Pb_i = 16{\cdot}6$–$16{\cdot}8$ and $17{\cdot}1$–$17{\cdot}4$; Fig. 8). There is, however, no obvious geographical control on the Pb isotope variations. Samples from individual locations may define part of one group (Loman, Murun, Verhni-Yakokut) or both groups (Nizhni-Yakokut). Samples from both Pb isotope groupings come from both the Central Aldan and Olekma Blocks. Equally there is no coherent regional variation to Th/U, μ ($^{238}U/^{204}Pb$) or κ ($^{232}Th/^{204}Pb$) ratios (Table 4). These data, therefore, indicate that there was local heterogeneity in the mantle source enrichment processes that occurred over the entire region.

The relatively unradiogenic Pb isotope ratios of the Aldan lamproites plot to the left of the geochron on a $^{206}Pb/^{204}Pb$ vs $^{207}Pb/^{204}Pb$ isotope diagram (Fig. 8), implying a multi-stage history for their mantle source region. In addition, the Aldan samples define a linear array on the $^{207}Pb/^{204}Pb$ vs $^{206}Pb/^{204}Pb$ diagram (Fig. 8a) that has a slope equivalent to an age of ~3·0 Ga. The simplest interpretation of the Aldan Pb isotope data is that they represent a two-stage history. Estimates of the Bulk Earth Pb isotope composition can be modelled by single-stage evolution with a μ value of 8·99. Hence we assume initial evolution within a Bulk Earth reservoir (μ = 8·99) followed by fractionation at 3·0 Ga. Subsequent evolution requires second-stage μ values between 6·4 and 8·0 (Fig. 8). Irrespective of whether the slope of the data has age significance, the data clearly establish long-term evolution of the sources with different but low time-integrated U/Pb. Similar interpretations have been proposed for other lamproite occurrences (Fraser *et al.*, 1985; Murphy *et al.*, 2002). The simplest interpretation of the Pb isotope data is that the source region was initially part of the asthenospheric upper mantle that was subsequently subjected to marked trace element enrichment and incorporated into the lithosphere. More complex multi-stage models are possible (for example, also involving some evolution in a trace element depleted source), but the Pb data do not require such complexity. The Archaean age of the lamproite source implied by the Pb–Pb isotope data is consistent with the Nd and Hf model ages. Given the potential for parent–daughter fractionation during melting, the consistency of the age information is striking.

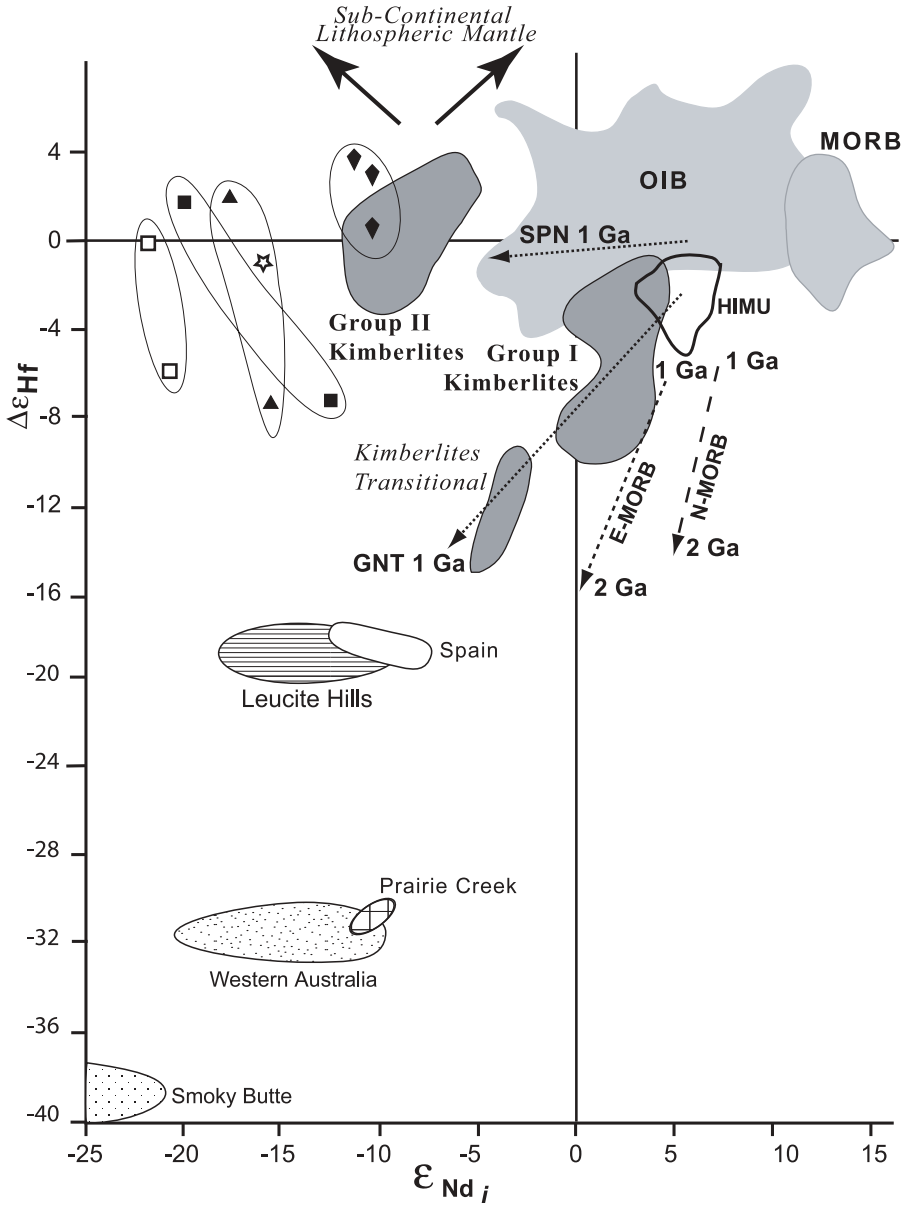

Fig. 7. Variation of $\Delta\varepsilon_{Hf}$ vs initial ε_{Nd} for Aldan lamproites and representative southern African Group I, Group II and Transitional kimberlites and examples of lamproites worldwide (Nowell *et al.*, 1998*a*, 2004). $\Delta\varepsilon_{Hf}$ is a measure of the difference of the Hf isotope composition from the mantle array ($\Delta\varepsilon_{Hf} = 0$), with data plotting above the reference line having positive $\Delta\varepsilon_{Hf}$ values. Data sources are as in Fig. 6. Dotted lines record the calculated temporal evolution of the isotopic composition of 1% non-modal batch partial melts of garnet (GNT) and spinel (SPN) facies peridotites up to 1 Ga. Starting source composition has ε_{Nd} of +7·5 and $\Delta\varepsilon_{Hf} = 0$. Source modes for calculation: garnet peridotite: olivine 0·6, orthopyroxene 0·15, clinopyroxene 0·15 and garnet 0·1, with a melting mode of 0·1:0·3:0·6:0·02. Spinel peridotite: olivine 0·65, orthopyroxene 0·15 and clinopyroxene 0·20, with a melting mode of 0·1:0·3:0·6. Partition coefficients are taken from Johnson (1998). Dashed lines marked N-MORB and E-MORB indicate the predicted change in isotopic composition of oceanic crust recycled at 1·0 and 2·0 Ga, respectively. Lu/Hf and Sm/Nd ratios of MORB and E-MORB are taken from Hofmann (1988) and Rehkämper & Hofmann (1997). Filled black arrows pointing towards sub-continental lithospheric mantle indicate the position of worldwide SCLM peridotite xenoliths. Data are from Salters & Zindler (1995), Ionov & Weis (2002), Schmidburger *et al.* (2002) and Simon *et al.* (2002).

Trace element enrichment: source enrichment or magmatic fractionation?

A notable feature of the Aldan Shield lamproites is that, compared with other lamproites, they have low abundances of moderately compatible trace elements such as the middle REE and LREE. The degree of trace element enrichment is up to an order of magnitude less than for other lamproite occurrences (Fig. 3). There are two alternative explanations for this difference in enrichment: (1) the source of the Aldan samples was less enriched, or

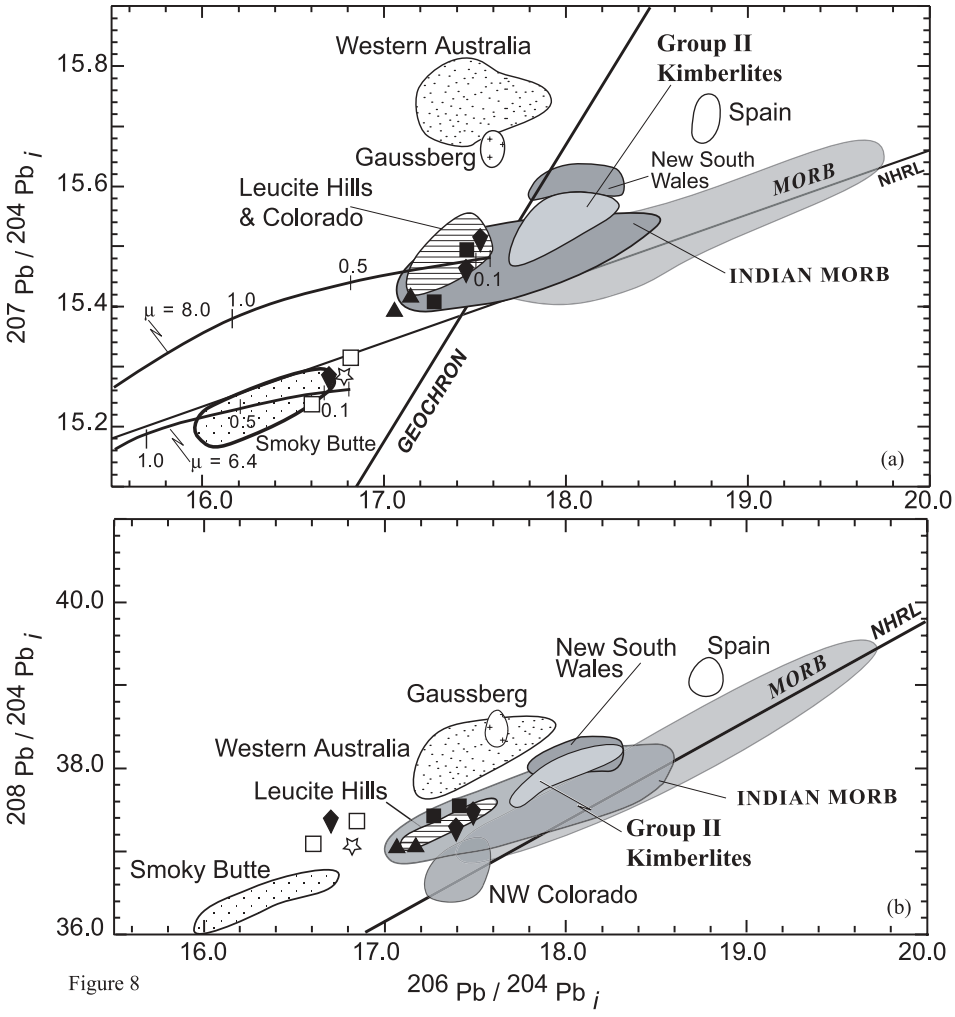

Figure 8

Fig. 8. Initial $^{206}Pb/^{204}Pb$ vs (a) $^{207}Pb/^{204}Pb$ and (b) $^{208}Pb/^{204}Pb$ for the Aldan lamproites and representative worldwide lamproites and southern African kimberlites. Combined fields for Atlantic and Pacific MORB and for Indian MORB are also shown for comparison. Data are from Hofmann (1997) and references therein. Lamproite and kimberlite data sources are as in Fig. 5. The Northern Hemisphere Reference Line (NHRL) is from Hart (1984). The entire Pb isotope dataset of the Aldan lamproites defines a slope equivalent to an age of 3·0 Ga. Model two-stage Pb–Pb evolution lines are shown for reference assuming an initial μ value of 8·99 until 3·0 Ga and then subsequent evolution with second-stage μ values of 6·4 and 8, respectively. Tick marks on the evolution lines represent 0·1, 0·5 and 1·0 Ga in the past.

(2) lamproite sources worldwide have undergone different degrees of partial melting. The discussion of the Sm–Nd and U–Th–Pb isotope systematics above clearly established that the Nd and Pb model ages are broadly comparable. The Nd isotope ratios are among the least radiogenic initial ratios measured in mantle-derived magmas, indicating long-term and marked LREE enrichment of the mantle source. Measured μ values are predominantly between 1·4 and 4·7, with only two samples having a present-day μ above 10. Measured κ ratios are also low, mostly between 2·6 and 11·4, with the same two samples again having higher ratios (Table 4). Measured Th/U are between 1·9 and 2·7, with only two samples (3·8–3·9) approaching the estimated Bulk Earth value of ~4·2 (Allègre *et al.*, 1986). The low measured parent/daughter ratios are consistent with the low time-integrated Th/U and U/Pb values inferred from the Pb isotope ratios. These data are indicative of the style of trace element enrichment in the source region and imply marked relative Pb enrichment. Th/Pb ratios must have been enriched to a greater extent than U/Pb to explain the relatively high $^{208}Pb/^{204}Pb$. The measured parent/daughter ratios are generally equal to, or lower than, those inferred from the time-integrated Pb isotope ratios. This is a surprising observation given that U and Th are generally considered to be more incompatible in the mantle during partial melting. Consequently, we conclude that the melting event that produced the lamproites did not significantly increase the parent/daughter ratios. From this observation there are two possible

Table 4: Pb isotope compositions of the Aldan Shield lamproites

Sample	Age(Ma)	U	Th	Pb	μ	κ	$^{206}Pb/^{204}Pb_m$	$^{207}Pb/^{204}Pb_m$	$^{208}Pb/^{204}Pb_m$	$^{206}Pb/^{204}Pb_i$	$^{207}Pb/^{204}Pb_i$	$^{208}Pb/^{204}Pb_i$
424/85	143	1·116	2·086	55·8	1·396	2·629	16·753	15·282	37·283	16·722	15·280	37·26
495/85	143	0·786	2·092	14·21	3·924	10·521	17·496	15·464	37·507	17·408	15·460	37·43
116/84	143	1·333	2·92	24·9	3·802	8·389	17·505	15·478	37·557	17·420	15·474	37·50
19/86	136	1·123	2·57	7·33	10·875	25·069	17·492	15·421	37·589	17·260	15·409	37·42
101/86	136	1·422	3·89	26·4	3·825	10·540	17·494	15·470	37·566	17·412	15·466	37·49
126/86	122	0·325	0·875	5·41	4·218	11·439	17·131	15·402	37·195	17·050	15·398	37·13
127/86	122	0·208	0·789	5·31	2·755	10·256	17·215	15·421	37·206	17·162	15·418	37·14
132/86	133	3·30	6·48	3·54	67·012	132·55	18·005	15·312	38·094	16·608	15·243	37·22
136/86	133	1·60	6·20	62·4	1·795	7·006	16·810	15·312	37·385	16·773	15·310	37·34
68/88	120	5·65	12·51	84·0	4·702	10·487	16·842	15·287	37·285	16·754	15·283	37·22

m, measured ratios; i, initial ratios.

conclusions: (1) residual phases preferentially retained Th and U, or (2) the melting degree was sufficiently great (>5%) that U/Pb and Th/Pb were not significantly increased compared with their source. In addition, the fractionated HREE ($Dy/Yb_n \sim 2$) suggest that at some stage during lamproite petrogenesis garnet was a residual phase. Fractionated HREE are a characteristic of all lamproites except those from Spain. The Spanish lamproites have high HREE contents ($Yb_n = 10–15$) that are not markedly fractionated and hence imply derivation from the spinel stability field (Nixon *et al.*, 1984).

Experimental evidence suggests that lamproites are in equilibrium with an assemblage that contains phlogopite, richterite, clinopyroxene, apatite and minor phases such as K–Ba–HFSE-rich titanites at pressures up to 3 GPa (Mitchell, 1995; Edgar & Mitchell, 1997; Konzett *et al.*, 1998; Foley *et al.*, 1999). During partial melting such a residual mineralogy has the potential to cause marked trace element fractionation between melt and residue. Evidence of trace element fractionation by residual phases has been widely reported. For example, the effect of residual phlogopite has been invoked to explain the trace element signature of melilitites and basanites from South Africa and East Africa (e.g. Rogers *et al.*, 1992).

The primitive mantle normalized trace element characteristics of the Aldan lamproites (Fig. 3) show relative LILE enrichment with no evidence to suggest that there was a residual K-rich phase in the source (i.e. relative K depletion). In detail, however, the LILE record marked variations that imply a complex source mineralogy. For example, K/Rb ratios vary between 170 and 420, Rb/Ba from 0·01 to 0·19 and Rb/Sr from 0·04 to 0·5. These ratios span almost the entire range recorded by lamproites worldwide (e.g. Fraser *et al.*, 1985). Typical mantle minerals do not cause fractionation in trace element ratios such as Rb/Ba and most mantle-derived magmas have Rb/Ba of ~0·05. Lamproites often have lower values, suggesting a role for residual phlogopite, which has a $D_{Rb/Ba}$ up to three [e.g. see review by Nixon & Davies (1987)]. In contrast, K-rich amphiboles have lower $D_{Rb/Ba}$ by up to two orders of magnitude. The variability of the Aldan lamproite samples, with Rb/Ba between 0·03 and 0·19, suggests highly variable input of potassic phases to the melt. The highly variable Rb/Sr ratios (0·04–0·51) of the Aldan lamproites also support this conclusion. High Rb/Sr and Rb/Ba are interpreted as the signatures of a mica-rich source, whereas low Rb/Sr and Rb/Ba are interpreted as indicating an amphibole-rich source.

The ancient nature of the LILE fractionation in the source of the Aldan lamproites is emphasized by the correlations between LILE and Sr isotope ratios (Fig. 9). For example, K and Rb contents have positive correlations with $^{87}Sr/^{86}Sr$ ($r^2 = 0·666$ and 0·214, respectively), whereas Cs/Rb has a negative correlation ($r^2 = 0·734$). Other elements mobile in volatile-rich environments (e.g. U and Ba) also record positive correlations with $^{87}Sr/^{86}Sr$ but, as with the Sr–Nd–Pb isotope data, there are two groups of samples that are not simply related to sample locality (Fig. 9). These data again stress the importance of LILE-rich phases such as amphibole and phlogopite in the genesis of the Aldan lamproites. The elevated U and Pb concentrations of the rocks, coupled with high LILE, suggest that volatile-rich melts were probably involved in the genesis of these lamproites. In addition, source regions were characterized by at least two distinct compositions. The first source has relatively low K_2O, Rb, Ba, U and $^{87}Sr/^{86}Sr$ and high Cs/Rb, whereas the second source has the opposite characteristics.

The apparently contradictory conclusions that residual K-rich phases have not fractionated the trace element

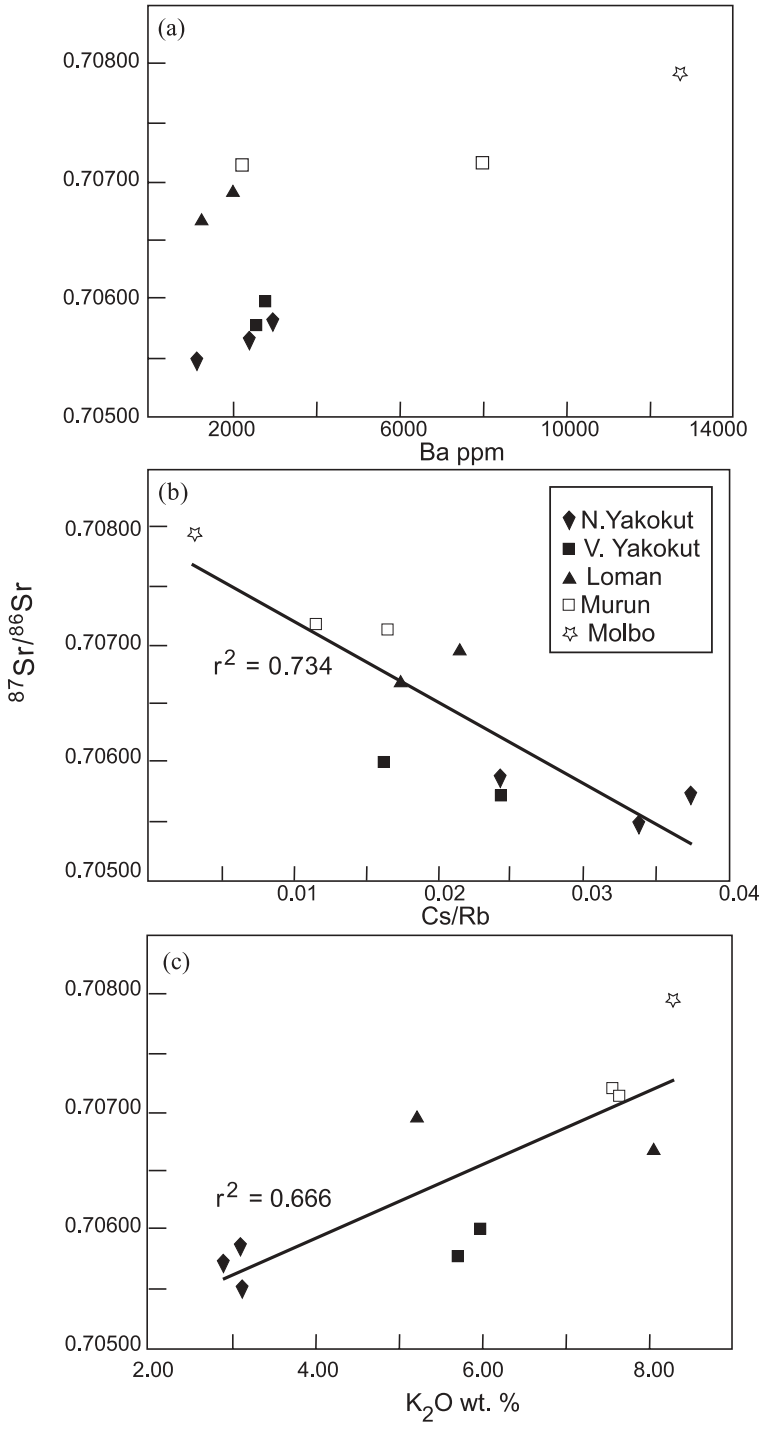

Fig. 9. Sr isotope variations of the Aldan lamproites plotted against (a) Ba contents, (b) Cs/Rb and (c) K_2O wt %. Symbols are as in Fig. 2.

composition of the Aldan lamproites, but that phlogopite and amphibole have contributed to the LILE budget, argues for extensive melting of the source such that the K-rich phases were exhausted. This conclusion is consistent with the moderate degree of LREE enrichment discussed above. Hydrous pyroxenite assemblages frequently contain apatite and minor phases such as K–Ba–HFSE-rich titanites that could potentially fractionate the U/Th/Pb ratios. The high Pb contents of the Aldan lamproites, however, argue against these phases being

residual and responsible for the low U/Pb and Th/Pb ratios. In addition, the low measured U/Pb ratios of the lamproites are consistent with the low time-integrated Pb isotope ratios. We, therefore, conclude that the Aldan lamproites were derived by large degrees of melting of phlogopite–amphibole-bearing peridotites or hydrous pyroxenitic vein assemblages within peridotites (e.g. Foley *et al.*, 1999). Furthermore, the melts have not undergone extensive trace element fractionation during melt extraction so that they may retain many trace element characteristics of their source.

A negative $\Delta\varepsilon_{Hf}$ signature

The Aldan lamproites have ε_{Hf}–ε_{Nd} signatures that range from these comparable with Group II kimberlites to more unradiogenic values (Fig. 6). The majority of the Aldan lamproites plot close to the mantle array in the ε_{Hf} vs ε_{Nd} diagram but three samples plot significantly below the array, with $\Delta\varepsilon_{Hf}$ values more negative than −5 (Fig. 7). Five samples have positive $\Delta\varepsilon_{Hf}$ values (+0·3 to +3·4; Table 3). The data used to define the MORB–OIB mantle array, however, have significant scatter and the positive values of the Aldan lamproites are within the range of modern oceanic basalts (e.g. Vervoort *et al.*, 1999). Lamproites worldwide are characterized by similarly unradiogenic Nd and Hf isotope ratios to the Aldan samples (Nowell *et al.*, 1998*a*) but are characterized by more markedly negative $\Delta\varepsilon_{Hf}$ values (–16 to −40). A negative $\Delta\varepsilon_{Hf}$ value therefore appears to be a characteristic of most lamproites.

The negative $\Delta\varepsilon_{Hf}$ signature of most lamproites and some kimberlites requires that their mantle source regions had, relative to the sources of MORB and OIB that define the mantle array, a time-integrated decoupling of Lu/Hf and Sm/Nd. The isotopic ratios require a greater lowering of Lu/Hf than Sm/Nd so that over time the isotopic ratios evolve to Hf isotope ratios below the mantle array. The terms f_{Sm} and f_{Lu} are used to quantify the fractionation of parent/daughter ratios (Sm/Nd and Lu/Hf) relative to the chondritic ratio (Patchett *et al.*, 1984; see Fig. 10 for definition). Despite not having extreme $\Delta\varepsilon_{Hf}$, the high-quality trace element dataset from the Aldan lamproites may provide the key to understanding the processes responsible for the fractionation of Sm/Nd and Lu/Hf. With the exception of sample 126/86, Aldan lamproites have f_{Lu} and f_{Sm} values that define a weak positive trend with a correlation coefficient of 0·45 (Fig. 10a). f_{Lu} is greater than f_{Sm}, as is required to generate the time-integrated negative $\Delta\varepsilon_{Hf}$ signatures. The correlations between f_{Lu}–f_{Sm} and f_{Lu}–$\Delta\varepsilon_{Hfi}$ (Fig. 10b) indicate that the major fractionation recorded in the source rocks occurred in the Archaean and that partial melting has not greatly fractionated the REE relative to the HFSE, again arguing for a relatively large degree of melting.

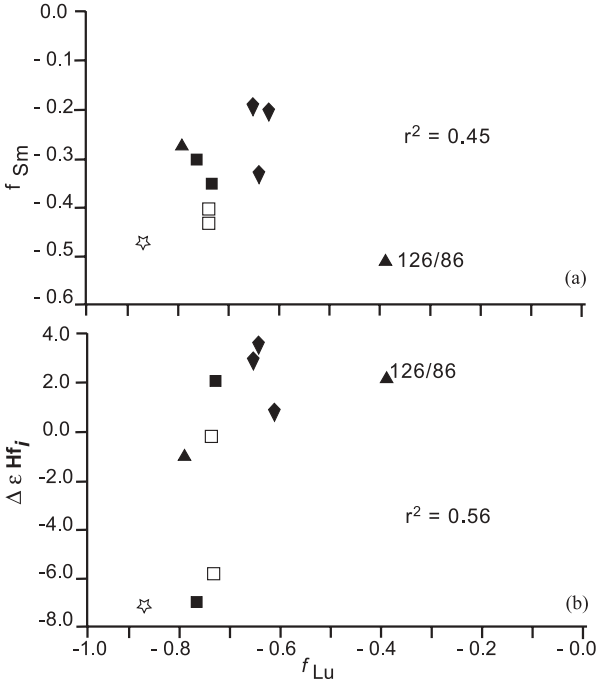

Fig. 10. Diagrams of f_{Lu} plotted against (a) f_{Sm} and (b) $\Delta\varepsilon_{Hf}$. f_{Lu} and f_{Sm} are used to quantify the fractionation of ratios relative to the chondritic ratio; for example, $f_{Sm} = [(^{147}Sm/^{144}Nd)/(^{147}Sm/^{144}Nd)_{CHUR}] - 1$.

Previous reports of mantle-derived melts with negative $\Delta\varepsilon_{Hf}$ values are relatively rare and represent rocks of two distinct petrogenetic types. First, HIMU OIB from islands with characteristic radiogenic Pb isotope ratios, such as St Helena and Tubuaii have $\Delta\varepsilon_{Hf}$ values as low as −7 (Fig. 7; e.g. Chauvel *et al.*, 1992; Salters & White, 1998). Similar characteristics occur in both the oceanic and continental sectors of the Tertiary Cameroon Volcanic Line (Ballentine *et al.*, 1997) and in olivine melilitites from South Africa (Janney *et al.*, 2002). Significantly, however, HIMU basalts have characteristic trace element contents that include high U/Pb and relatively low LILE contents (i.e. low LILE/LREE and LILE/HFSE), clearly distinct from the Aldan Shield lamproites. In addition, the HIMU basalts are characterized by relatively radiogenic ε_{Nd} values in the range +3 to +6. A source for the Aldan lamproites directly comparable with the source of HIMU OIB is, therefore, unlikely. Southern African Group I kimberlites also have negative $\Delta\varepsilon_{Hf}$ values, −9·7 being the most extreme value reported to date (Nowell *et al.*, 1998*a*, 1999, 2004). Bizzarro *et al.* (2002) have reported negative $\Delta\varepsilon_{Hf}$ values from zircons and baddeleyite mineral separates from Archaean carbonatites that yielded discordant U–Pb ages. In this case, however, the required age corrections are so large that it is difficult to unambiguously interpret the results as consistently recording a negative $\Delta\varepsilon_{Hf}$ signature.

Two mantle source components have been proposed to explain the origin of negative $\Delta\varepsilon_{Hf}$ signatures: subcratonic lithospheric mantle and recycled subducted oceanic crust (e.g. Ballentine *et al.*, 1997; Salters & White, 1998; Nowell *et al.*, 1998*a*, 2004; Griffin *et al.*, 2000; Janney *et al.*, 2002). It is beyond the scope of this study to revisit this subject in detail, and only a brief summary is provided here. The fundamental observation made by all previous workers is that melts in equilibrium with garnet-bearing residua exhibit greater Lu/Hf fractionation than Sm/Nd, such that with time the crystallization products of these melts will evolve, over time periods in excess of 1 Gyr, to isotopic compositions below the Nd–Hf isotope array with negative $\Delta\varepsilon_{Hf}$ (Figs 6 and 7). Consequently, long-term storage of such melt fractions (e.g. as veins within the lithospheric mantle) will produce a source with negative $\Delta\varepsilon_{Hf}$ values. Modelling has demonstrated that storage of melts derived from MORB-source mantle will produce steep evolution lines in an Hf–Nd isotope diagram, retaining positive ε_{Nd} (e.g. Ballantine *et al.*, 1997; Fig. 7). More trace element enriched melts, e.g. E-MORB, will evolve with a slightly less steep slope on this diagram, approaching Bulk Earth ε_{Nd} values ($\sim$0) after $>$2 Gyr (e.g. Nowell *et al.*, 2004). Although capable of explaining the negative $\Delta\varepsilon_{Hf}$ values of Group I kimberlites, these models do not explain the extreme negative ε_{Nd} values of lamproites (Figs 6 and 7).

The SCLM is potentially a mantle source with negative $\Delta\varepsilon_{Hf}$ values. This reservoir has been shown by numerous workers to have remained isolated for billions of years (e.g. see review by Pearson, 1999) and to have been affected by numerous and different styles of metasomatic trace element enrichment (e.g. Harte, 1983; Nixon & Davies, 1987; Pearson, 1999). Combined Nd–Hf isotope data on mantle samples from the SCLM remain relatively limited; however, the available data (Ionov & Weis, 2002; Schmidburger *et al.*, 2002; Simon *et al.*, 2002) consistently reveal markedly radiogenic Hf isotope ratios with positive $\Delta\varepsilon_{Hf}$ values up to 350. These data imply that a time-integrated signal of Lu/Hf depletion is widely preserved in the SCLM, but that a time-integrated signal of Sm/Nd depletion is often overprinted by subsequent LREE enrichment. Previous studies indicate that the vast majority of the SCLM appears to have initially been formed by extensive melt extraction (e.g. Pearson, 1999) but to have subsequently been modified by trace element enrichment processes close to the time of transport of mantle xenoliths (samples of the SCLM) to the surface by kimberlitic magmatism (e.g. Simon *et al.*, 2003). As such, mantle xenoliths are unlikely to represent the source of trace element enriched magmas and, hence, are not expected to explain lamproite trace element and isotopic compositions. To date, the majority of SCLM samples studied for Hf isotopes are depleted in basaltic components. However, time-integrated ratios can be inferred from more fertile sources using available trace element data and melting models. Small-degree melts ($\sim$1%) derived from the spinel stability field would have small negative $\Delta\varepsilon_{Hf}$ values after 17 Gyr storage (~-2, Fig. 7). In contrast, $\sim$1% partial melts derived from the garnet stability field have extremely low f_{Lu} values such that negative $\Delta\varepsilon_{Hf}$ values of ~-14 would be produced after 1 Gyr storage (Fig. 7). Highly metasomatized mantle xenoliths, such as the MARID suite and phlogopite–K-richterite peridotites, have combined f_{Sm} and f_{Lu} values that would produce negative $\Delta\varepsilon_{Hf}$ values over time (e.g. Nowell *et al.*, 2004). Metasomatism of the SCLM by melts derived from the garnet stability field, therefore, appears a possible explanation of the source of those Aldan lamproites that have negative $\Delta\varepsilon_{Hf}$ and strongly negative ε_{Nd} and ε_{Hf}.

Nature and origin of HFSE fractionation

The origin of the relative HFSE depletion is perhaps the key to understanding the petrogenesis of the majority of the Aldan lamproitic rocks. Figure 3a demonstrates that the HFSE are more depleted than elements with a comparable degree of incompatibility during mantle melting. For example, Zr and Hf have lower normalized contents than Sm. Isovalent HFSE pairs such as Zr–Hf and Nb–Ta have similar ionic radii and, as such, should behave similarly during partial melting processes. Consequently, many workers have regarded the Nb/Ta and Zr/Hf ratios of most of the major silicate reservoirs in the Earth to be constant and approximately chondritic. Chondritic Nb/Ta and Zr/Hf ratios are 17·6 and 34·2–36·6, respectively (Jochum *et al.*, 1986; Weyer *et al.*, 2003). Until recently, resolvable fractionation of the HFSE ratio pairs Nb/Ta and Zr/Hf was difficult to assess. The introduction of new, externally calibrated, analytical techniques such as spark source mass spectrometry (Jochum *et al.*, 1990) and ICP-MS, particularly isotope dilution ICP-MS (Weyer *et al.*, 2002), has demonstrated that, despite the expected similar chemical behaviour, some mantle processes can fractionate Nb/Ta and Zr/Hf ratios. Super-chondritic Zr/Hf ratios have been recognized in metasomatized peridotite xenoliths and OIB (e.g. Ionov *et al.*, 1993; David *et al.*, 2000). Sub-chondritic Zr/Hf and Nb/Ta occur in depleted MORB, peridotites and komatiites (Weyer *et al.*, 2003, and references therein). The most significant variations in Nb/Ta occur in highly potassic subduction-related rocks (e.g. Indonesian olivine leucitites have Nb/Ta up to 34, Stolz *et al.*, 1996); understanding the genesis of these extreme values may help understand the HFSE fractionation recorded in the Aldan lamproites.

The published Nb/Ta ratios of Group II kimberlites and lamproites are in the range 12–24 (e.g. Turner *et al.*, 1999; Wannamaker *et al.*, 2000; Murphy *et al.*, 2002).

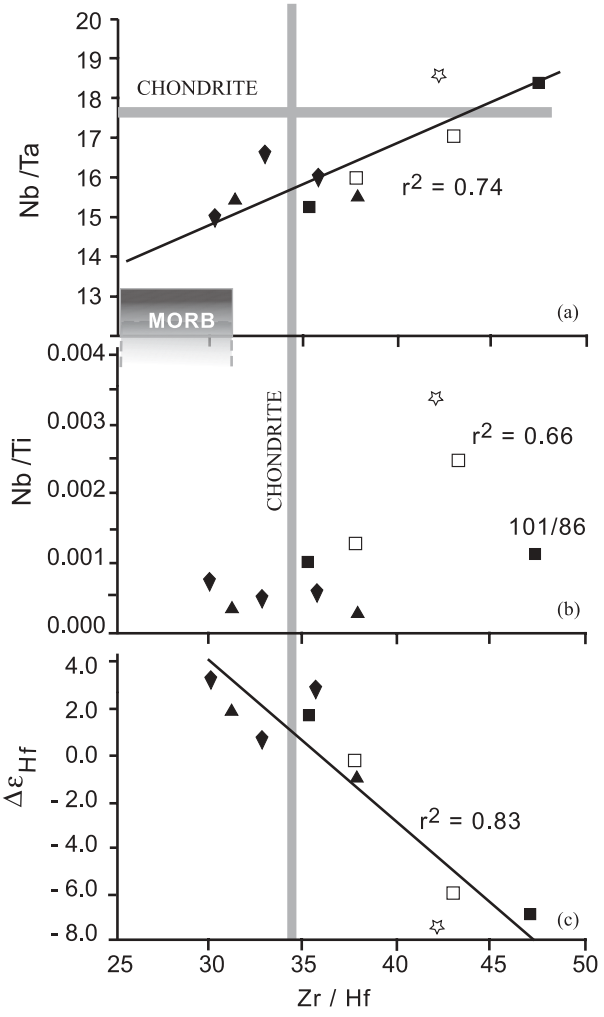

Fig. 11. Zr/Hf vs (a) Nb/Ta, (b) Nb/Ti and (c) $\Delta\varepsilon_{Hf}$.

Given that these data have not been determined by the most modern analytical techniques, it is unclear if the variations are actually significantly different from the chondritic value of 17·6. The high-precision HFSE data for the Aldan lamproites record significant variations in Nb/Ta (14·7–18·2) and Zr/Hf (30·6–47·4), extending to both higher and lower values than the chondritic ratios (17·6 and ~35, respectively). There is a good correlation between Nb/Ta and Zr/Hf with an r^2 of 0·74 (Fig. 11a), suggesting that a common process fractionated these trace elements. The importance of the above observations is that published Zr–Hf and Nb–Ta partition coefficients, although variable, generally predict that during mantle melting Hf and Nb are slightly more compatible than Zr and Ta, respectively (Hart & Dunn, 1993; Blundy *et al.*, 1998; Johnson, 1998; Lundstrom *et al.*, 1998; Salters & Longhi, 1999; Klein *et al.*, 2000). D_{Zr}/D_{Hf} for clinopyroxene is ~0·5 in the spinel stability field. In contrast, D_{Zr}/D_{Hf} for clinopyroxene is close to unity in the garnet stability field. The experimentally determined partition coefficients were recently confirmed by a study of depleted mantle peridotites from the Balmuccia Complex (Weyer *et al.*, 2003). Nb/Ta ratios in the Balmuccia peridotites are predominantly in the range 7–10, comparable with those of N-MORB. These data imply that Nb is more incompatible than Ta during partial melting in the mantle, which is consistent with the relative Nb–Ta fractionation predicted by the experimental studies cited above.

However, the predicted magnitude of Nb/Ta and Zr/Hf fractionation under melting conditions controlled by typical residual mantle mineralogies is small, and unlikely to produce the variation observed in the Aldan lamproites. HFSE depletion and inter-element fractionation is characteristic of many lamproites and subduction zone magmas, where some of the most extreme Nb/Ta ratios are observed (Indonesian olivine leucitites, Nb/Ta >30; Stolz *et al.*, 1996). It is useful therefore, to examine the processes that contribute to Indonesian magmatism so as to understand better the origin of the trace element fractionation in lamproites. It is important to recognize that subducted sediments in the Indonesian region have sub-chondritic Nb/Ta ratios (Vroon *et al.*, 1995) and, thus, sediment subduction cannot be the explanation for the high Nb/Ta ratios of the Indonesian olivine leucitites.

One model invoked to explain HFSE depletion in subduction-related magmas and lamproites requires a role for residual rutile and amphibole during slab dehydration or melting (Nicholls & Ringwood, 1973; Mitchell & Bergman, 1991). Both minerals have high, but distinct, mineral–melt and mineral–fluid partition coefficients (D <100) for Nb and Ta, with Ta having the higher D value (e.g. Green *et al.*, 1989; Adam *et al.*, 1993; Brenan *et al.*, 1994; Stadler *et al.*, 1998). Rutile–fluid partition coefficients are so high for all HFSE that there will be little net HFSE flux from a slab resulting from dehydration reactions that occur during slab subduction. Ti-bearing phlogopite would also contribute to HFSE fractionation during dehydration and partial melting processes. Currently, however, partition coefficients for this phase are not well constrained; consequently, we concentrate our arguments below on rutile and amphibole. Significant Zr/Hf and Nb/Ta fractionation in subduction zone magmas will be recorded only if HFSE fluxes are large enough to overprint the depleted HFSE ratios of the overlying mantle wedge. This was the reasoning used by Stolz *et al.* (1996) to explain the different Nb/Ta ratios of low- and high-K magmas in the Indonesian Arc. Slab dehydration was suggested to generate large-degree melts from the mantle wedge that were characterized by low Nb/Ta ratios. Slab-derived melts are, however, also required to cause marked inter-element fractionation in the source regions of the

Indonesian high-K leucitites (Stolz *et al.*, 1996). Slab melting will leave residua with low Nb/Ta ratios. The high Nb/Ta of Indonesian high-K olivine leucitites requires very large elemental fractionation and implies >1% residual rutile (Stolz *et al.*, 1996). Residual slabs are therefore predicted to have low Nb/Ta and Zr/Hf ratios. This conclusion is the opposite to that of Rudnick *et al.* (2000), who suggested that, on average, rutile-bearing eclogites recycled into the mantle have high Nb/Ta ratios. The explanation of this dichotomy is probably that the rutile-bearing eclogites from Sierra Leone studied by Rudnick and coworkers (e.g. Barth *et al.*, 2001) represent Archaean slab-derived melts that have undergone a complex petrogenesis during storage in the SCLM that included multiple episodes of melting. These eclogites are, therefore, interpreted as modified slab-derived melts that infiltrated the SCLM, rather than portions of a subducted slab tectonically emplaced into the SCLM. This explanation is consistent with the experimentally determined HFSE partition coefficients and does not require that we ignore a large experimental database, which suggests that Nb is more incompatible during melting of all important mantle minerals at variable P, T and melt composition (e.g. Green *et al.*, 1989; Hart & Dunn, 1993; Brenan *et al.*, 1994; Adam *et al.*, 1993; Blundy *et al.*, 1998; Johnson, 1998; Lundstrom *et al.*, 1998; Stadler *et al.*, 1998; Salters & Longhi, 1999; Klein *et al.*, 2000; Foley *et al.*, 2000).

The Aldan lamproites exhibit correlations between Zr/Hf, Nb/Ta and Nb/Ti (Fig. 11a and b) strongly suggesting a role for rutile and amphibole in their petrogenesis. If present, rutile would be the major Ti- and Nb-bearing phase in any mantle assemblage. Other trace element ratios expected to be fractionated by rutile also record significant correlations, e.g. Zr/Sm or Lu/Hf vs Nb/Ta (not shown; see Table 2). The Aldan lamproites have inter-HFSE ratios that vary from sub- to superchondritic (e.g. Zr/Hf and Nb/Ta; Fig. 11). The subchondritic Zr/Hf and Nb/Ta ratios of some Aldan samples suggest that one component of the source was melt-depleted. HFSE ratios also show general correlations with the Nd–Hf–Pb isotope data. For example, Zr/Hf and Nb/Ta have positive and negative correlations with $^{208}Pb/^{206}Pb$ and ε_{Hf}, respectively (Tables 2 and 3). These correlations clearly establish that the HFSE fractionation was ancient and probably that the protolith had depleted trace element characteristics prior to enrichment (e.g. a low Nb/Ta ratio). $\Delta\varepsilon_{Hf}$ is strongly correlated ($r^2 \sim 0{\cdot}7$–$0{\cdot}8$) with Zr/Hf, Nb/Ta and Nb/Ti (Fig. 11). These relationships provide strong support for the suggestion that ancient rutile ± amphibole-controlled fractionation was responsible for the decoupling of the Nd–Hf isotope ratios. The preservation of correlations between trace element ratios and time-integrated parent/daughter ratios emphasizes that the trace element enrichment of the source, and not partial melting, was the major factor that controlled the present-day trace element abundances of the lamproites. Moreover, the role of rutile ± amphibole ± phlogopite in controlling the trace element composition of the Aldan lamproites suggests that their formation may have been in a subduction-related tectonic environment. This conclusion is in agreement with the conclusion reached above that melting of K-rich hydrous phases was responsible for controlling the LILE budget of these lamproites.

The combined trace element and isotopic systematics of the Aldan lamproites are compatible with derivation from a source region that has been variably enriched during the Archaean by hydrous melts, forming a hydrated peridotite or hydrous pyroxenite veins in a depleted protolith. The style of trace element enrichment in the Aldan lamproites is comparable with that of high-K subduction-related magmas. Numerous estimates have been made concerning the nature of the fluids and melts responsible for trace element enrichment in the source of subduction-related magmas. All studies have concluded that the sources of medium- to high-K magmas are significantly enriched in LILE and that there is variable LREE enrichment but no evidence of HREE (Lu) enrichment (e.g. Tatsumi *et al.*, 1986; Pearce & Parkinson, 1993; Stolz *et al.*, 1996; Gertisser & Keller, 2003). The sources of the Aldan lamproites appear to record the addition of hydrous silicate melts, possibly derived from subducted slabs, to a depleted mantle protolith and are consistent with an important role for residual garnet and rutile.

Source composition

We have argued above, based on their major and trace element geochemistry, that the Aldan lamproites were relatively large-degree partial melts of a metasomatized mantle source. The dominant metasomatic mineral assemblages recorded in mantle xenoliths derived from the SCLM are amphibole- and mica- bearing, but also include a variety of minor phases such as ilmenite, rutile and apatite (e.g. Harte 1983; Nixon & Davies, 1987). The most extreme manifestations are amphibole–mica pyroxenite veins. Such mineral assemblages have low solidus temperatures and should produce a large melt fraction close to their solidus (e.g. Foley *et al.*, 1999). There is sufficient experimental work on the melting of such materials over a range of P–T conditions to assess if this conclusion is reasonable (e.g. Foley, 1991; Sweeney *et al.*, 1993; Foley *et al.*, 1999). These experiments have shown that amphibole provides the dominant control on melt generation. Melt compositions are primarily controlled by the composition of the amphibole. K-richterite breaks down incongruently, forming olivine and clinopyroxene, whereas pargasite breaks down in the presence of apatite

to form clinopyroxene. Melts of K-richterite-bearing assemblages are rich in SiO_2 and K_2O and poor in CaO and Al_2O_3; in some respects these melts are similar to leucite lamproites (Foley *et al.*, 1999). This observation is consistent with the proposal that lamproites are derived by melting of veins in the SCLM (Mitchell, 1995). In detail, however, the starting compositions in the melting experiments were highly variable, particularly with respect to the proportions of minor phases, and did not yield liquids identical in composition to lamproites. Such compositional differences are, however, to be expected because of the extreme heterogeneity of vein compositions in the SCLM and the certainty that melts derived from hydrous pyroxenites would react with the peridotite wall-rock and thus become modified in composition. The fact that such extreme magma compositions are erupted emphasizes that once melt has separated from the residuum it must quickly form into channels and be rapidly transported to the surface.

The model proposed here for lamproite generation is similar to that proposed for subduction-related K-rich magmas (e.g. Stolz *et al.*, 1990; Rogers, 1992; van Bergen *et al.*, 1992). The styles of trace element enrichment and HFSE fractionation appear comparable. Shoshonites typically have higher SiO_2, Al_2O_3 and CaO contents than lamproites and lower K/Al ratios. This observation is consistent with experimental studies that show that melting of pargasitic amphibole-bearing pyroxenite will produce melts with lower K/Al and generally higher CaO contents than K-richterite-bearing assemblages. The derivation of subduction-related shoshonitic magma from somewhat shallower depths than lamproites could explain the major element differences between these two types of high-K magmas.

Implications for lamproite petrogenesis

The Pb isotope data provide strong constraints on the possible source of the Aldan lamproites, particularly in the context of their derivation from a sub-lithospheric or a SCLM source (Fig. 8). Lamproites from Western Australia and Spain are characterized by markedly higher $^{208}Pb/^{206}Pb$ and $^{207}Pb/^{206}Pb$ ratios than Atlantic OIB, such that researchers have argued for the involvement of recycled sediments in their source (e.g. Nelson, 1992; Turner *et al.*, 1999). The Pb isotope compositions of the Aldan lamproites could, potentially, be used to argue for the involvement of a small component of recycled sediment; however, long-term storage of a mantle source with elevated Th/Pb and Th/U is an equally plausible explanation. In the context of distinguishing between an SCLM and a sub-lithospheric mantle source, an important observation is that the Aldan lamproites have less radiogenic $^{206}Pb/^{204}Pb$ than all present-day MORB and OIB (Fraser *et al.*, 1985). The importance of this observation is that the isotopic signatures of many OIB define mixing relationships with MORB (e.g. Hart, 1984; Abouchami *et al.*, 2000), implying that the end-member compositions of OIB sources are not necessarily recorded in OIB. Consequently, the Pb isotope compositions of almost all end-member sources of OIB are likely to be more radiogenic than the OIB spectrum. The fact that the Aldan lamproites have less radiogenic Pb isotope ratios than MORB only emphasizes the differences between OIB and the lamproites. Any mixing with partial melts of MORB source mantle would tend to increase, not decrease, the Pb isotope ratios of the lamproites. The Pb isotope compositions of the lamproites, therefore, provide no evidence for derivation from a sub-lithospheric OIB-like source. The Sr–Nd isotope compositions of lamproites worldwide are also highly variable, suggesting that each of the source regions has a unique history (Fig. 5). Significantly, no lamproite source regions have Sr–Nd isotope compositions comparable with present-day oceanic magmatism, again suggesting that there is no connection between plume-related OIB-like sources and lamproite sources. Furthermore, Pearson *et al.* (1996) have reported highly radiogenic Os isotope compositions for many lamproites, consistent with derivation from a metasomatized sub-continental lithospheric mantle source.

Several workers have argued for a sub-lithospheric origin for both kimberlites (Le Roex, 1986) and lamproites (Murphy *et al.*, 2002). Le Roex (1986) cited chemical similarities between OIB and kimberlites in support of a sub-lithospheric origin for kimberlites. Murphy *et al.* (2002) have argued, based on a study of Gaussberg lamproites, that lamproites are derived from the Transition Zone (>400 km depth) where subducted sediments are stored. Part of their argument is that OIB and lamproites have distinct isotopic signatures but that enriched OIB sources do not contain recycled sedimentary components. This conclusion is in contradiction to the findings of numerous workers who have cited extensive evidence for the presence of recycled sedimentary material in the source of OIB (see, e.g. reviews by Hofmann, 1997; Davies *et al.*, 1989, and more recent contributions by Rehkämper & Hofmann, 1997; Blichert-Toft *et al.*, 1999; Eiler *et al.*, 2000). Therefore, although acknowledging that there is compelling evidence that the sources of the Aldan and some other lamproites may contain a component of recycled oceanic crust, including sediment, there appear to be no data to support derivation of this component from deep within the asthenosphere. Long-term storage in the SCLM appears a more feasible explanation for a slab-derived signature.

Further evidence for the importance of subduction-related processes in lamproite genesis can be found by consideration of elements with similar degrees of incompatibility during silicate melting but different behaviour

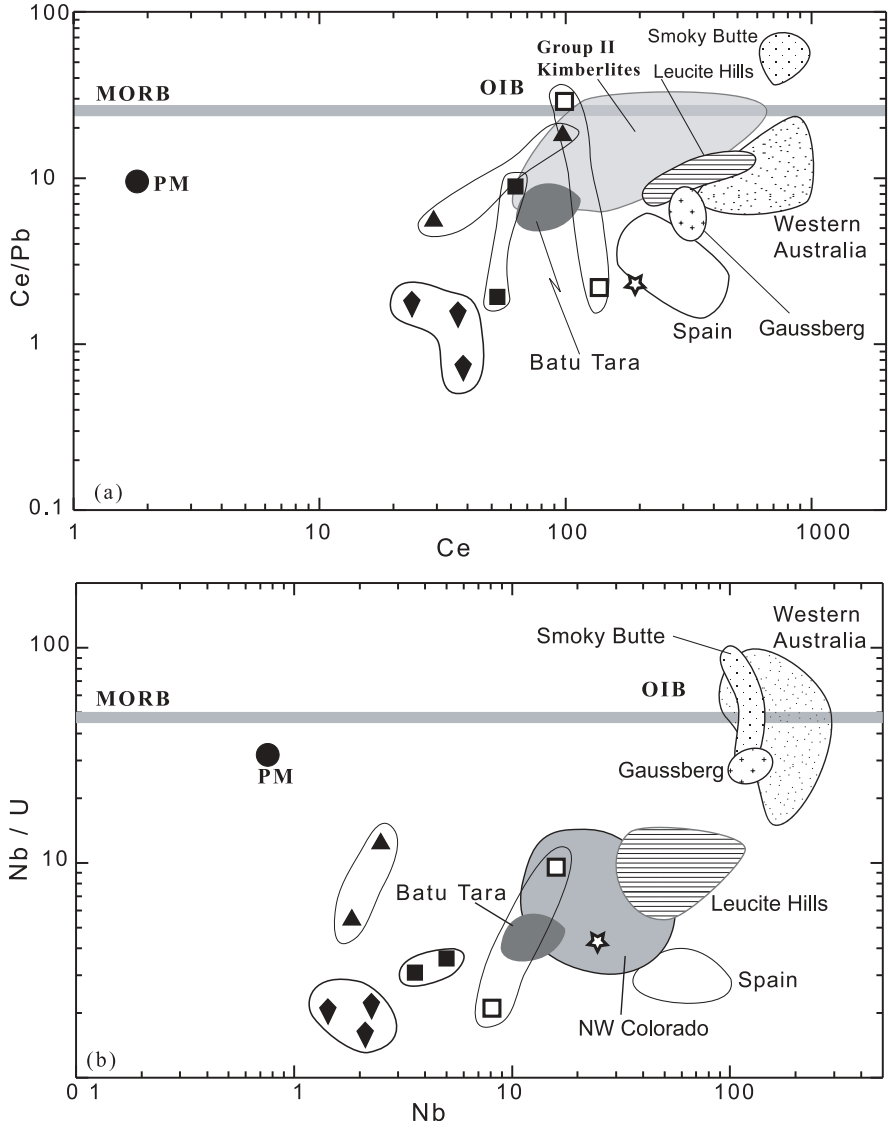

Fig. 12. Variation of (a) Ce/Pb vs Ce and (b) Nb/U vs Nb. Primitive Mantle (PM), MORB and OIB values are from Hofmann *et al.* (1986). Lamproite data sources are as in Fig. 4.

when fluid is present (e.g. Nb/U, Ce/Pb; Hofmann *et al.*, 1986). The enrichment of the source of the Aldan lamproites has resulted in low Nb/U (<10) and Ce/Pb as low as 0·7 (Fig. 12); these ratios correlate with HFSE ratios (e.g. Ce/Pb vs Zr/Hf, Table 2). These data clearly imply hydrous melt-related source enrichment. Although the trace element datasets for other lamproite suites are not complete, the available data suggest that hydrous melt enrichment of the source is not ubiquitous. For example, Group II kimberlites, and Western Australian and Smoky Butte lamproites have Nb/U ratios comparable with present-day MORB and OIB (Fig. 12; Fraser *et al.*, 1985; Jacques *et al.*, 1986). Lamproites from Spain and the Leucite Hills have high Zr/Ti ratios and low Ce/Pb and Nb/U ratios (Fig. 12). These characteristics are more comparable with those of subduction-related magmas than the Western Australian lamproites, and previous workers have concluded that subduction-related processes played an important role in their genesis (Fraser *et al.*, 1985; Nelson *et al.*, 1986; Turner *et al.*, 1999). Unfortunately, to date, there are few high-quality Nb/Ta and Zr/Hf data for other lamproites. Hence it is difficult to assess, unequivocally, if subduction-related processes involving residual rutile and/or amphibole are the cause of the trace element enrichment of the source of all lamproites. The Gaussberg lamproites have Nb/Ta ratios that are both sub- and super-chondritic (17–20), and Murphy *et al.* (2002) used this fact as part of the reasoning for invoking subduction-related processes in their petrogenesis.

CONCLUSIONS

Extension-related, Mesozoic, ultrapotassic, ultrabasic lamproites from the Aldan Shield have a number of chemical characteristics that are distinct from those of other lamproites worldwide. There are, however, more similarities than differences, suggesting that models for the genesis of Aldan lamproites may be applicable to other lamproites. The Aldan lamproites have among the most extreme isotopic ratios yet recorded from mantle-derived magmas. Given the potential for parent–daughter isotope fractionation during mantle melting, the consistency of the Archaean ages derived from the Nd–Hf and Pb isotope data is striking, and provides strong evidence that melt extraction involved a sufficiently large degree of melting that it did not disrupt isotope–trace element correlations. This conclusion explains the relatively low LREE contents of the lamproites and the coherent variations between trace element and isotopic ratios. Some of the Aldan lamproites are characterized by negative $\Delta\varepsilon_{Hf}$ values (+3 to −7). The origin of this signature has been the subject of much recent debate (e.g. Ballentine *et al.*, 1997; Salters & White, 1998; Nowell *et al.*, 1999, 2004; Bizzarro *et al.*, 2002; Janney *et al.*, 2002). Examination of HFSE fractionation provides the key to understanding the origin of this signature and the ultimate petrogenesis of the Aldan lamproites. Strong correlations between Nb/Ta, Zr/Hf and Nb/Ti establish an important role for residual rutile ± amphibole in the enrichment processes that produced the source of the Aldan lamproites. In addition, ε_{Hf} and $\Delta\varepsilon_{Hf}$ correlate with Lu/Hf and HFSE ratios (e.g. Nb/Ta). Together, these variations indicate that the HFSE fractionation occurred in the Archaean and led to the variable enrichment of a previously depleted source. The source enrichment is so old that it is impossible to use the isotopic data to assess whether recycled sediments were involved. Although high-quality trace element data (e.g. HFSE) are not available for most lamproites, it appears that many of their source regions contain a component of recycled oceanic crust, possibly including sediment. The sources of the Aldan and many other lamproites are distinct from all present-day plume-related OIB-like mantle sources. This strongly suggests that long-term storage of the trace element enriched lamproite mantle sources occurred in the SCLM and not at depth within the convecting asthenosphere.

ACKNOWLEDGEMENTS

A.J.S. acknowledges receipt of a Humboldt fellowship that allowed this study to be initiated during stays at MPI Mainz. Guidance in the laboratories and discussions with Klaus-Pieter Jochum, Al Hofmann, Steve Galer and Wafa Abouchami were invaluable. The initial manuscript benefited from discussion with Pieter Vroon and Tim Elliott. Constructive formal reviews by Janne Blichert-Toft, Phil Janney and Balz Kamber were most helpful in improving the focus of the manuscript. Marjorie Wilson was responsible for prompt, thorough and incisive editorial handling of the manuscript.

REFERENCES

Abouchami, W., Galer, S. J. G. & Hofmann, A. W. (2000). High precision lead isotope systematics of lavas from the Hawaiian Scientific Drilling Project. *Chemical Geology* **169**, 187–209.

Adam, J., Green, T. H. & Sie, S. H. (1993). Proton microprobe determined partitioning of Rb, Sr, Ba, Y, Zr, Nb and Ta between experimentally produced amphiboles and silicate melts with variable F content. *Chemical Geology* **109**, 29–49.

Allègre, C. J., Dupré, B. & Lewin, E. (1986). Thorium/uranium ratio of the Earth. *Chemical Geology* **56**, 219–227.

Ballentine, C. J., Lee, D.-C. & Halliday, A. N. (1997). Hafnium isotopic studies of the Cameroon Line and new HIMU paradoxes. *Chemical Geology* **139**, 111–124.

Barth, M. G., Rudnick, R. L., Horn, I., McDonough, W. F., Spicuzza, M. J., Valley, J. W. & Haggerty, S. E. (2001). Geochemistry of xenolithic eclogites from West Africa, part I: A link between low MgO eclogites and Archean crust formation. *Geochimica et Cosmochimica Acta* **65**, 1499–1527.

Beard, B. L. & Johnson, C. M. (1993). Hf isotope composition of late Cenozoic basaltic rocks from northwestern Colorado, USA: new constraints on mantle enrichment processes. *Earth and Planetary Science Letters* **119**, 495–509.

Bergman, S. C. (1987). Lamproites and other potassium-rich igneous rocks; a review of their occurrence, mineralogy and geochemistry. In: Fitton, J. G. & Upton, B. G. J. (eds) *Alkaline Igneous Rocks. Geological Society, London, Special Publications* **30**, 103–190.

Bilanenko, V. A., Spector, V. B. & Perfyonov, L. M. (1984). Geological outline of the Yakutsk ASSR. In: *Yakutsk ASSR Siberian Platform. Guidebook of Geology Conventus in Moscow 1984*, pp. 136–151.

Bizzarro, M., Simonetti, A., Stevenson, R. K. & David, J. (2002). Hf isotope evidence for a hidden mantle reservoir. *Geology* **30**, 771–774.

Blichert-Toft, J. & Albarède, F. (1997). The Lu–Hf isotope geochemistry of chondrites and the evolution of the mantle–crust. *Earth and Planetary Science Letters* **148**, 243–258.

Blichert-Toft, J., Frey, F. A. & Albarède, F. (1999). Hf isotope evidence for pelagic sediments in the source of Hawaiian basalts. *Science* **285**, 879–882.

Blundy, J. D., Robinson, J. A. C. & Wood, B. J. (1998). Heavy REE are compatible in clinopyroxene on the spinel lherzolite solidus. *Earth and Planetary Science Letters* **160**, 493–504.

Bogatikov, V. A., Machotkin, I. L. & Kononova, V. A. (1985). Lamproites and their place in the systematics of high-magnesium potassic rocks. *Proceedings of the Russian Academy of Sciences* **12**, 3–10.

Brenan, J. M., Shaw, H. F., Phinney, D. L. & Ryerson, F. J. (1994). Rutile–aqueous fluid partitioning of Nb, Ta, Hf, Zr, U and Th: implications for high field strength element depletions in island-arc basalts. *Earth and Planetary Science Letters* **128**, 327–339.

Chauvel, C., Hofmann, A. W. & Vidal, P. (1992) HIMU-EM: the French-Polynesian connection. *Earth and Planetary Science Letters* **110**, 99–119.

David, K., Schiano, P. A. & Allègre, C. J. (2000). Assessment of Zr/Hf fractionation in oceanic basalts and continental materials during petrogenetic processes. *Earth and Planetary Science Letters* **178**, 285–301.

Davies, G. R., Norry, M. J., Gerlach, D. C. & Cliff, R. A. (1989). A combined chemical and Pb–Sr–Nd isotope study of the Azores and Cape Verde hot spots: the geodynamic implications. In: Saunders, A. D. & Norry, M. J. (eds) *Magmatism in the Ocean Basins. Geological Society, London, Special Publications* **42**, 231–256.

Davies, G. R., Spriggs, A. J. & Nixon, P. (2001). A non-cognate origin for the Gibeon kimberlite megacryst suite, Namibia: implications for origin of Namibian kimberlites. *Journal of Petrology* **42**, 159–172.

Edgar, A. D. & Mitchell, R. H. (1997). Ultra high pressure–temperature melting experiments on a SiO_2-rich lamproite from Smoky Butte, Montana: derivation of siliceous lamproite magmas from enriched sources deep in the continental mantle. *Journal of Petrology* **38**, 457–477.

Eggins, S. M., Woodhead, J. D., Kinsley, L. P. J., Mortimer, G. E., Sylvester, P., McCulloch, M. T., Hergt, J. M. & Handler, M. R. (1997). A simple method for the precise determination of >40 trace elements in geological samples by ICPMS using enriched isotope internal standardisation. *Chemical Geology* **134**, 311–326.

Eiler, J. M., Schaino, J. M., Kitchen, N. & Stolper, E. M. (2000). Oxygen-isotope evidence for recycled crust in the source of mid-ocean-ridge basalts. *Nature* **403**, 530–534.

Foley, S. F. (1991). High pressure stability of the fluor- and hydroxy-end members of pargasite and K-richterite. *Geochimica et Cosmochimica Acta* **55**, 2689–2694.

Foley, S. F., Venturelli, G., Green, D. H. & Toscani, L. (1987). The ultrapotassic rocks: characteristics, classification and constraints for petrogenetic models. *Earth-Science Reviews* **24**, 81–134.

Foley, S. F., Musselwhite, D. S. & van der Laan, S. R. (1999). Melt compositions from ultramafic vein assemblages in the lithospheric mantle: a comparison of cratonic and non-cratonic settings. In: Gurney, J. J., Gurney, J. L., Pascoe, M. D. & Richardson, S. H. (eds) *Proceedings of the 7th International Kimberlite Conference*. Cape Town: Red Roof Design, pp. 238–246.

Foley, S. F., Barth, M. G. & Jenner, G. A. (2000). Rutile/melt partition coefficients for trace elements and an assessment of the influence of rutile on the trace element characteristics of subduction zone magmas. *Geochimica et Cosmochimica Acta* **64**, 933–938.

Fraser, K. J., Hawkesworth, C. J., Erlank, A. J., Mitchell, R. H. & Scott-Smith, B. H. (1985). Sr, Nd and Pb isotope and minor element geochemistry of lamproites and kimberlites. *Earth and Planetary Science Letters* **76**, 57–70.

Gertisser, R. & Keller, J. (2003). Trace element and Sr, Nd, Pb and O isotope variations in medium-K and high-K rocks from Merapi Volcano, Central Java, Indonesia: evidence for the involvement of subducted sediments in Sunda Arc magma genesis. *Journal of Petrology* **44**, 457–490.

Green, T. H., Sie, S. H., Ryan, C. G. & Cousens, D. R. (1989). Proton microprobe determined partitioning of Nb, Ta, Zr, Sr and Y between garnet, clinopyroxene and basaltic magma at high pressure and temperature. *Chemical Geology* **74**, 201–216.

Griffin, W. L., Pearson, N. J., Belousova, E., Jackson, S. E., van Achterbergh, E., O'Reilly, S. Y. & Shee, S. R. (2000). The Hf isotope composition of cratonic mantle: LAM–MC–ICPMS analysis of zircon megacrysts in kimberlites. *Geochimica et Cosmochimica Acta* **64**, 133–148.

Hart, S. R. (1984). A large-scale anomaly in the Southern Hemisphere mantle. *Nature* **309**, 753–757.

Hart, S. R. & Dunn, T. (1993). Experimental cpx/melt partitioning of 24 trace elements. *Contributions to Mineralogy and Petrology* **113**, 1–8.

Harte, B. (1983). Mantle peridotites and process—the kimberlite sample. In: Hawkesworth, C. J. & Norry, M. J. (eds) *Continental Basalts and Mantle Xenoliths*. Nantwich, Shiva: pp. 46–91.

Heumann, A. & Davies, G. R. (2002). A combined U–Th, Sr–Nd–Pb–O isotope study of the Navaisha comendite complex; implications for petrogenesis and magma chamber residence. *Journal of Petrology* **43**, 557–577.

Hofmann, A. W. (1988). Chemical differentiation of the Earth: the relationship between mantle, continental crust and oceanic crust. *Earth and Planetary Science Letters* **90**, 297–314.

Hofmann, A. W. (1997). Mantle geochemistry: the message from oceanic volcanism. *Nature* **385**, 219–229.

Hofmann, A. W., Jochum, K. P., Seufert, M. & White, W. M. (1986). Nb and Pb in oceanic basalts: new contraints on mantle evolution. *Earth and Planetary Science Letters* **97**, 33–45.

Ionov, D. A. & Weis, D. (2002) Hf–Nd–Sr isotope relationships in spinel and garnet facies peridotite xenoliths: inferences for the age and evolution of the lithospheric mantle. *Geochimica et Cosmochimica Acta* **66**, A356.

Ionov, D. A., Dupuy, C., O'Reilly, S. Y., Kopylova, M. G. & Genshaft, Y. S. (1993). Carbonated peridotite xenoliths from Spitsbergen: implications for trace element signature of mantle carbonate metasomatism. *Earth and Planetary Science Letters* **119**, 282–297.

Jaques, A. L., Lewis, J. D. & Smith, C. B. (1986). Kimberlites and lamproites of Western Australia. *Geological Survey Western Australia, Bulletin* **132**, 268.

Jahn, B.-M., Gruau, G., Capdvila, R., Cornichet, J., Nemchin, A., Pidgeon, R. & Rudnil, V. A. (1998). Archaean crustal evolution of the Aldan Shield, Siberia: geochemical and isotopic constraints. *Precambrian Research* **91**, 333–363.

Janney, P. E., Le Roex, A. P., Carlson, R. W. & Viljoen, K. S. (2002). A chemical and multi-isotope study of the Western Cape olivine melilitite province, South Africa: implications for the source of kimberlites and the origin of HIMU signature in Africa. *Journal of Petrology* **43**, 2339–2370.

Jochum, K. P., Seufert, H. M., Spettel, B. & Palme, H. (1986). The solar system abundances of Nb, Ta and Y, and the relative abundances of refractory lithophile elements in differentiated planetary bodies. *Geochimica et Cosmochimica Acta* **50**, 1173–1183.

Jochum, K. P., Seufert, H. M. & Thirlwall, M. F. (1990). High-sensitivity Nb analysis by spark-source mass spectrometry (SSMS) and calibration of XRF Nb and Zr. *Chemical Geology* **81**, 1–16.

Johnson, T. M. (1998). Experimental determination of partition coefficients for rare earth and high- field-strength elements between clinopyroxene, garnet and basaltic melt at high pressures. *Contributions to Mineralogy and Petrology* **133**, 60–68.

Klein, M., Stosch, H. G., Seck, H. A. & Shimizu, N. (2000). Experimental partitioning of high field strength and rare earth elements between clinopyroxene and garnet in andesitic to tonalitic systems. *Geochimica et Cosmochimica Acta* **64**, 99–115.

Konzett, J., Armstrong, R. A., Sweeney, R. J. & Compston, W. (1998). The timing of MARID metasomatism in the Kaapvaal mantle: an ion probe study of zircons from MARID xenoliths. *Earth and Planetary Science Letters* **160**, 133–145.

Le Roex, A. P. (1986). Geochemical correlation between Southern African kimberlites and South Atlantic hot spots. *Nature* **324**, 243–245.

Lundstrom, C. C., Shaw, H. F., Ryerson, F. J., Williams, Q. & Gill, J. (1998). Crystal chemical control of clinopyroxene–melt partitioning in Di–Ab–An system: implications for elemental fractionation in the depleted mantle. *Geochimica et Cosmochimica Acta* **62**, 2849–2862.

Mahotkin, I. L., Arakelyan, M. M. & Vladykin, N. V. (1989). Age of the Aldan lamproite province. *Doklady Akademii Nauk SSSR* **306**, 703–707 (in Russian).

McCulloch, M. T., Jaques, A. L., Nelson, D. R. & Lewis, J. D. (1983). Nd and Sr isotopes in kimberlites and lamproites from Western Australia: an enriched mantle origin. *Nature* **302**, 400–403.

Mitchell, R. H. (1995). Melting experiments on a sanidine phlogopite lamproite at 4–7 GPa and their bearing on the sources of lamproitic magmas. *Journal of Petrology* **36**, 1455–1474.

Mitchell, R. H. & Bergman, S. C. (1991). *Petrology of Lamproites*. New York: Plenum, 447 pp.

Mitchell, R. H., Smith, C. B. & Vladykin, N. V. (1994). Isotopic composition of strontium and neodymium in potassic rocks of the Little Murun complex, Aldan Shield, Siberia. *Lithos* **32**, 243–248.

Mues-Schumacher, U., Keller, J., Konova, V. & Suddaby, P. (1995). Petrology and age determinations of the ultramafic (lamproitic) rocks from the Yakokut complex, Aldan Shield, Eastern Siberia. *Mineralogical Magazine* **59**, 409–428.

Murphy, D. T., Collerson, K. D. & Kamber, B. S. (2002). Lamproites from Gaussberg, Antarctica: possible Transition Zone melts of Archaean subducted sediments. *Journal of Petrology* **43**, 981–1001.

Nelson, D. R. (1992). Isotopic characteristics of potassic rocks—evidence for the involvement of subducted sediments in magma genesis. *Lithos* **28**, 403–420.

Nelson, D. R., McCulloch, M. T. & Sun, S. S. (1986). The origins of ultrapotassic rocks as inferred from Sr, Nd and Pb isotopes. *Geochimica et Cosmochimica Acta* **50**, 231–245.

Nicholls, I. A. & Ringwood, A. E. (1973). Effect of water on olivine stability in tholeiites and production of silica-saturated magmas in the island-arc environment. *Journal of Geology* **81**, 285–300.

Nixon, P. H. & Davies, G. R. (1987). Mantle xenolith perspectives. In: Nixon, P. H. (ed.) *Mantle Xenoliths*. Chichester: John Wiley, pp. 741–756.

Nixon, P. H., Thirwall, M. F., Buckley, F. & Davies, C. J. (1984). Spanish and Western Australian lamproites: aspects of whole rock geochemistry. In: Kornprobst, J. (ed.) *Kimberlites and Related Rocks*. Amsterdam: Elsevier, pp. 285–296.

Nowell, G. M., Pearson, D. G., Kempton, P. D., Irving, A. J. & Turner, S. (1998*a*). A Hf isotope study of lamproites: implications for their origins and relationship to Kimberlites. In: *Extended Abstracts, 7th International Kimberlite Conference*. Cape Town: University of Cape Town, pp. 637–639.

Nowell, G. M., Kempton, P. D., Noble, S. R., Fitton, J. G., Saunders, A. D., Mahoney, J. J. & Taylor, R. N. (1998*b*). High precision Hf isotope measurements of MORB and OIB by thermal ionisation mass spectrometry: insights into the depleted mantle. *Chemical Geology* **149**, 211–233.

Nowell, G. M., Pearson, D. G.,Kempton, P. D., Noble, S. R. & Smith, C. B. (1999). Origins of Kimberlites: a Hf isotope perspective. In: Gurney, J. J., Gurney, J. L., Pascoe, M. D. & Richardson, S. H. (eds) *Proceedings of the 7th International Kimberlite Conference*. Cape Town: Red Roof Design, pp. 616–624.

Nowell, G. M., Pearson, D. G., Ottley, C. J., Schwieters, J. & Dowall, D. (2003). Long-term performance of a plasma ionisation multi-collector mass spectrometer (PIMMS): the ThermoFinnigan Neptune. In: Holland, J. G. & Tanner, S. D. (eds) *Plasma Source Mass Spectrometry: Applications and Emerging Technologies*. Cambridge: The Royal Society of Chemistry, pp. 307–320.

Nowell, G. M., Pearson, D. G., Bell, D., Carlson, R., Smith, C., Kempton, P. & Noble, S. (2004). Hf isotope systematics of kimberlites and their megacrysts: new constraints on their source regions. *Journal of Petrology* **45**, 1583–1612.

Panina, L. I. (1997). Low-titanium Aldan lamproites (Siberia): melt inclusions in minerals. *Russian Geology and Geophysics* **38**, 118–127.

Patchett, P. J., White, W. M., Feldmann, H., Kielinezuk, S. & Hofmann, A. W. (1984). Hafnium/rare earth element fractionation in sedimentary system and crustal recycling into the Earth's mantle. *Earth and Planetary Science Letters* **69**, 365–378.

Pearce, J. A. & Parkinson, I. J. (1993). Trace element models for mantle melting: application to volcanic arc petrogenesis. In: Prichard, H. M., Alabaster, T., Harris, N. B. W. & Neary, C. R. (eds) *Magmatic Processes and Plate Tectonics*. *Geological Society, London, Special Publications* **76**, 373–403.

Pearson, D. G. (1999). The age of continental roots. *Lithos* **48**, 171–194.

Pearson, D. G., Snyder, G. A. & Shirley, S. B. (1995). Archean Re–Os age for Siberian eclogites and constraints on Archean tectonics. *Nature* **374**(6524), 711–713.

Pearson, D. G., Rogers, N. W., Irving, A. J., Smith, C. B. & Hawkesworth, C. J. (1996). Re–Os isotope constraints on the sources of kimberlites and lamproites. *Journal of Conference Abstracts* **1**, 453.

Pearson, D. G., Shirley, S. B., Bulanova, G. P., Carlson, R. W. & Milledge, H. J. (1999). Re–Os isotope measurements of single inclusions in a Siberian diamond and its nitrogen aggregation systematics. *Geochimica et Cosmochimica Acta* **63**, 703–711.

Perchuk, L. L., Aranivich, L. Y., Podlesskiy, K. K., Lavrant, I. V., Gerasimov, V. Y., Fedkin, V. V., Kitsul, V. I., Karsakov, L. P. & Berdnikov, N. V. (1985). Precambrian granulites of the Aldan Shield, Eastern Siberia. *Journal of Metamorphic Geology* **3**, 265–310.

Popov, N. V. & Smelov, A. P. (1996). The Aldan Shield metamorphic assemblages. *Russian Geology and Geophysics* **37**, 148–161.

Rehkämper, M. & Hofmann, A. W. (1997). Recycled ocean crust and sediment in Indian Ocean MORB. *Earth and Planetary Science Letters* **147**, 93–106.

Rogers, N. (1992). Potassic magmatism as a key to trace-element enrichment processes in the upper mantle. *Journal of Volcanology and Geothermal Research* **50**, 85–99.

Rogers, N., Hawkesworth, C. J. & Palacz, Z. A. (1992). Phlogopite in the generation of olivine-melilitites from Namaqualand, South Africa and implications for element fractionation processes in the upper mantle. *Lithos* **28**, 347–365.

Rosen, O. M., Serenko, V. P., Spetsius, Z. V., Manakov, A. V. & Zinchuk, N. N. (2002). Yakutian Kimberlite Province: position in the structure of the Siberian craton and composition of the upper and lower crust. *Russian Geology and Geophysics* **43**, 1–24.

Rudnick, R. L., Barth, M., Horn, I. & McDonough, W. F. (2000). Rutile-bearing refractory eclogites: missing link between continents and depleted mantle. *Science* **287**, 278–281.

Salters, V. J. M. & Longhi, J. (1999). Trace element partitioning during the initial stage of melting beneath mid-oceanic ridges. *Earth and Planetary Science Letters* **147**, 109–123.

Salters, V. J. M. & White, W. M. (1998). Hf isotope constraints on mantle evolution. *Chemical Geology* **145**, 447–460.

Salters, V. J. M. & Zindler, A. (1995). Extreme $^{176}Hf/^{177}Hf$ in the sub-oceanic mantle. *Earth and Planetary Science Letters* **129**, 13–30.

Schmidburger, S. S., Simonetti, A. & Francis, D. (2002) Probing Archean lithosphere using the Lu–Hf systematics of peridotite xenoliths from Somerset Island kimberlites, Canada. *Earth and Planetary Science Letters* **197**, 245–259.

Scott Smith, B. H. & Skinner, E. M. W. (1984). A new look at Prairie Creek, Arkansas. In: Kornprobst, J. (ed.) *Kimberlites I: Kimberlites and Related Rocks*. Amsterdam: Elsevier, pp. 255–283.

Simon, N. S. C., Carlson, R. W., Pearson, D. G. & Davies, G. R. (2002). The Lu–Hf isotope composition of cratonic lithosphere: disequilibrium between garnet and clinopyroxene in kimberlite xenoliths. *Geochimica et Cosmochimica Acta* **66**, A356.

Simon, N. S. C., Irvine, G. J., Davies, G. R., Pearson, D. G. & Carlson, R. W. (2003). The origin of garnet and clinopyroxene in 'depleted' Kaapvaal peridotites. *Lithos* **71**(2–4), 28–322.

Smith, C. B. (1983). Pb, Sr and Nd isotopic evidence for sources of Southern African Cretaceous Kimberlites. *Nature* **304**, 51–54.

Smith, C. B., Gurney, J. J., Skinner, E. M. W., Clement, C. R. & Ebrahim, N. (1985). Geochemical character of southern African kimberlites: a new approach based on isotopic constraints. *Transactions of the Geological Society of South Africa* **88**, 267–280.

Stadler, R., Foley, S. F., Brey, G. P. & Horn, I. (1998). Mineral–aqueous fluid partitioning of trace elements at 900–1200°C and 3·0–5·7 GPa: new experimental data for garnet, clinopyroxene and rutile and implications for mantle metasomatism. *Geochimica et Cosmochimica Acta* **62**, 1781–1801.

Stolz, A. J., Varne, R., Davies, G. R., Wheller, G. E. & Foden, J. D. (1990). Magma source components in an arc–continent collision zone: the Flores–Lembata sector, Sunda arc, Indonesia. *Contributions to Mineralogy and Petrology* **105**, 585–601.

Stolz, A. J., Jochum, K. P., Spettel, B. & Hofmann, A. W. (1996). Fluid- and melt-related enrichment in the subarc mantle: evidence from Nb/Ta variations in island-arc basalts. *Geology* **24**, 587–590.

Sun, S-s. & McDonough, W. F. (1989). Chemical and isotopic systematics of oceanic basalts: implications for mantle composition and processes. In: Saunders, A. D. & Norry, M. J. (eds) *Magmatism in the Ocean Basins*. *Geological Society, London, Special Publications* **42**, 313–345.

Sweeney, R. J., Thompson, A. B. & Ulmer, P. (1993). Phase relations of a natural MARID composition and implications for MARID genesis, lithospheric melting and mantle metasomatism. *Contributions to Mineralogy and Petrology* **115**, 225–241.

Tatsumi, Y., Hamilton, D. L. & Nesbitt, R. W. (1986). Chemical characteristics of fluid phase released from a subducted lithosphere and origin of arc magmas: evidence from high-pressure experiments and natural rocks. *Journal of Volcanology and Geothermal Research* **29**, 293–309.

Turner, S. R., Platt, J. P., George, R. M. M., Kelley, S. P., Pearson, D. G. & Nowell, G. M. (1999). Magmatism associated with orogenic collapse of the Betic–Alboran domain, SE Spain. *Journal of Petrology* **40**, 1011–1036.

Van Bergen, M. J., Vroon, P. Z., Varekamp, J. C. & Poorter, R. P. E. (1992). The origin of the potassic rock suite from Batu Tara volcano (East Sunda Arc, Indonesia). *Lithos* **28**, 261–282.

Vavilov, M. A., Bazarova, Y. T., Podgornykh, N. M., Krivoputskaya, L. M. & Kuznetsova, I. K. (1986). Characteristics and formation conditions of potassic alkaline rocks of the Loman Massif. *Russian Geology and Geophysics* **27**, 40–46.

Venturelli, G., Caspedri, S., Di Battistini, G., Crawford, A., Kogarko, L. N. & Celestini, S. (1984). The ultrapotassic rocks from southeastern Spain. *Lithos* **17**, 37–54.

Vervoort, J. D., Patchett, P. J., Blichert-Toft, J. & Albarède, F. (1999). Relationships between Lu–Hf and Sm–Nd isotopic systems in the global sedimentary system. *Earth and Planetary Science Letters* **168**, 79–99.

Vladykin, N. V. (1996). Bilibin massif—layered differentiated complex of K-ultrabasic–alkalic rocks. *Doklady Akademii Nauk SSSR* **349**, 703–707 (in Russian).

Vladykin, N. V. (1997). Geochemistry and genesis of lamproites of the Aldan Shield. *Russian Geology and Geophysics* **38**, 128–141.

Vroon, P., van Bergen, M. J., Klaver, G. J. & White, W. M. (1995). Strontium, neodymium and lead isotopic and trace element signatures of the East Indonesian sediments: provenance and implications for Banda Arc magma genesis. *Geochimica et Cosmochimica Acta* **59**, 1583–1595

Wannamaker, P. E., Hulen, J. B. & Heizler, M. T. (2000). Miocene lamproite from the Colorado Plateau tectonic province, Southeastern Utah, USA. *Journal of Volcanology and Geothermal Research* **96**, 175–190.

Weyer, S., Münker, C., Rehkamper, M. & Mezger, K. (2002). Determination of ultra low Nb, Ta, Zr and Hf concentrations and precise Nb/Ta and Zr/Hf ratios by isotope dilution analyses with multiple collector ICP-MS. *Chemical Geology* **187**, 295–313.

Weyer, S., Münker, C. & Mezger, K. (2003). Nb/Ta, Zr/Hf and REE in the depleted mantle: implications for the differentiation history of the crust–mantle system. *Earth and Planetary Science Letters* **205**, 309–324.

White, W. M. & Dupre, B. (1986). Sediment subduction and magma genesis in the Lesser Antilles: isotopic and trace element constraints. *Journal of Geophysical Research* **91**, 5927–5944.